01.72.

Instituto de Física "José A. Balseiro"

Universidad Nacional de Cuyo

Comisión Nacional de Energía Atómica

Calores Específicos de Superconductores con Impurezas Magnéticas

Tesis presentada ante la Universidad Nacional de Cuyo para optar al titulo de Doctor en Física

M. Brian Maple

Dr. M. Brian Maple

Asesor Científico

Carlos A. Luengo

Carlos A. Luengo

San Carlos de Bariloche (R. N.)

Argentina - 1972

A los que siempre me acompañan

Mis padres

Mis hermanos

Mis amigos

TABLE OF CONTENTS

LIST OF TABLES

LIST OF FIGURES

Page

Figures - Part II

ACKNOWLEDGMENTS

I am deeply indebted to M. Brian Maple for his guidance and continuous encouragement during the hardest stages of this research.

I am also very grateful to Al Sweedler for introducing me to the problem of magnetic impurities and for valuable discussions concerning my experiments, and to Daniel Thoulouze for teaching me the techniques of specific heat measurements.

During the years I spent at the Centro Atómico Bariloche (CAB) I enjoyed the friendship, collaboration and invaluable support of: Blas Alascio, Julián Sereni, Coco Cotignola, Marcel Locatelli, Paco de la Cruz, María Elena de la Cruz, Oscar J. Bressan, Alberto Ridner, Raul Rapp, Heriberto Tutzauer and Ricardo Scotti.

A good part of this work was done at the University of California, San Diego (UCSD). I wish to express my gratitude to Professor Bernd T. Matthias; he generously supported my work and provided a stimulating atmosphere in his laboratory. There, I have enjoyed the sympathy, advice and many times, the important collaboration of: John Huber, Dieter Wohlleben, Ana Celia Mota, R. Viswanathan, John Engelhardt, Fred Smith, Lance DeLong and William Fertig. I thank Ben Ricks and Nancy McLaughlin who provided important technical and secretarial assistance.

My visits to the Facultad de Ciencias in Santiago de Chile were invaluable to my professional and personal development. Along with Al Sweedler; Miguel Kiwi, Miguel Roth and Sergio Ortega have earned my gratitude both as physicists and friends.

I am thankful for the interest and advice of Professors Leo M. Falicov and Martin J. Zuckermann; they were especially encouraging to me during the early stages of this work.

The sharp criticism and strong support of Professor Enrique Gaviola have decisively influenced my formation as a physicist since my first year as an undergraduate. To him my deep appreciation.

Finally, I thank the John Simon Guggenheim Memorial Foundation, the Consejo Nacional de Investigaciones Científicas y Técnicas, and the Comisión Nacional de Energía Atómica (CNEA) for different fellowships.

This research was partly conducted at the CAB and at the Physics Department of UCSD; I acknowledge the financial assistance of the CNEA and the Air Force Office of Scientific Research, Air Force Systems Command, USAF, under AFOSR Contract #AFOSR/F-44620-72-C-0017.

VITA

August 12, 1943 - Born - Buenos Aires, Argentina

1962-1964	School of Engineering, University of Buenos Aires
1964-1967	Institute of Physics "José A. Balseiro" Bariloche, Argentina
1967	Licenciado en Física
1968-1971	Research Assistant, Centro Atómico Bariloche, Bariloche, Argentina
1968-1971	Instructor in Physics, Institute "José A. Balseiro"
1972	Research Visiting Fellow, Physics Department, University of California, San Diego, La Jolla, California
1964-1967	Argentine Atomic Energy Commission (CNEA) Scholarship
1968-1970	CNEA Research Fellowship
1971	Argentine National Research Council Fellowship
1971-1972	John Simon Guggenheim Memorial Foundation Fellowship

PUBLICATIONS

"Thermal and Electrical Conductivities of Very High Purity Indium," M. E. de la Cruz, F. de la Cruz, J. M. Cotignola, O. J. Bressan and C. A. Luengo, Phys. Rev. 176, 871 (1968)

"Low Temperature Specific Heats of β' and ξ_0 Phases in Equiatomic AgZn," J. Abriata, O. J. Bressan, C. A. Luengo, and D. Thoulouze, Phys. Rev. 2, 1464 (1970)

"On the Evidence for Electron-Electron Scattering in the Electrical Resistivity of Indium," O. J. Bressan, A. J. Ridner, C. A. Luengo, and Blas Alascio, Solid State Commun. 8, 2129 (1970)

"Low Temperature Specific Heat of ThU," C. A. Luengo, J. M. Cotignola, J. G. Sereni, A. R. Sweedler, M. B. Maple, and J. G. Huber, Solid State Commun. 10, 459 (1972)

"Heat Capacity of ThU at Low Temperature," C. A. Luengo, J. M. Cotignola, A. R. Sweedler, and M. B. Maple, Proceedings 13th Int. Conf. on Low Temp. Phys. (1972), to be published

"Specific Heat of the Superconducting-Kondo System (La, Ce)Al_2," C. A. Luengo, M. B. Maple, and W. Fertig, Solid State Commun. (forthcoming)

"The Specific Heat of the (La, Gd)Al_2 System in the Superconducting and Normal States," C. A. Luengo and M. B. Maple, to be published

FIELDS OF STUDY

Major Field: Physics

Studies in Low Temperature Solid State Physics
Centro Atómico Bariloche - Comisión Nacional de Energia Atómica - Argentina- and Physics Department, University of California, San Diego, California, U. S. A.

RESUMEN

Se ha medido el calor específico en los estados normal y superconductor de los sistemas ThU, (La, Gd)Al_2 y (La, Ce)Al_2, donde U, Gd y Ce son impurezas representativas de diferentes casos de magnetismo. A partir de los resultados de los experimentos se ha establecido la existencia de una relación directa entre la discontinuidad del calor específico ΔC a la temperature crítica T_c y la curva de T_c versus concentración n de impurezas para los diferentes comportamientos magnéticos de los sistemas mencionados.

En el sistema ThU, $\Delta C(T_c)$ depende linealmente de T_c de acuerdo a la ley de estados correspondientes de Bardeen, Cooper y Schrieffer (BCS); $\Delta C/\Delta C_o = T_c/T_{co}$; donde ΔC_o y T_{co} son ΔC y T_c para la matriz de Th. Esta dependencia corresponde con el comportamiento exponencial de la curva de T_c vs. n, que caracteriza a los sistemas débilmente magnéticos.

En (La, Gd)Al_2, los resultados experimentales indican que $\Delta C(T_c)$ y T_c estan relacionadas por la dependencia funcional predicha por la teoría de Abrikosov-Gor'kov (AG) para impurezas magnéticas, en estrecha vinculación con las mediciones de T_c vs. n

que también han indicado un buen acuerdo con los respectivos cálculos dentro del marco postulado por AG.

En (La, Ce)Al_2 se observa que $\Delta C(T_c)$ se desvía fuertemente de las predicciones teóricas de BCS y AG, lo que corresponde con las recientes determinaciones de la curva de T_c vs. n que presenta peculiares desviaciones de la teoría de AG debido al efecto Kondo.

El calor específico en el estado normal de los tres sistemas aumenta visiblemente, aún con pequenas fracciones de impurezas. En ThU, la variación del coeficiente γ del calor específico electrónico puede expresarse como $d\gamma/dn = 2.7$ mj/mole°K^2 at.% U para bajas concentraciones de U.

En (La, Ce)Al_2 la contribución magnética de las impurezas a la capacidad calorífica en el estado normal crece como (-ln T) entre 0.5 y 2.5 °K e indica la presencia de un máximo que debería ocurrir a temperaturas del orden de 0.1 °K que es la temperatura de Kondo de este sistema. Esta anomalía no es visiblemente afectada por campos magnéticos menores que $\sim$ 1.7 kgauss; en contraste, la capacidad calorífica de las aleaciones de (La, Gd)Al_2, depende fuertemente del campo externo aplicado sobre la muestra. Para campos pequeños varía como (-ln T) entre 0.5 y $\sim$ 3 °K.

El calor específico electrónico es también extremadamente sensible a pequeñas concentraciones de Ce y Gd; $\Delta\gamma = 0.37$ joule/

mole $Gd°K^2$ para $(\underline{La}, Ce)Al_2$ y $(\underline{La}, Gd)Al_2$ respectivamente. También en estos dos sistemas los efectos de impurezas son visibles en el calor específico del estado superconductor hasta temperaturas mucho menores que T_c .

Los experimentos se hicieron en calorímetros semi-adiabáticos de simple diseño. Se presentan y describen brevemente sus principales características.

ABSTRACT

The heat capacities of ThU, (La, Gd)Al_2 and (La, Ce)Al_2 alloys were measured in the superconducting and normal states.

A phenomenological correspondence is established between the behavior of the specific heat jump ΔC at the superconducting critical temperature T_c and the previously known, detailed dependence of T_c on impurity concentration n for the aforementioned magnetically distinct matrix-impurity systems. For the ThU system the reduced specific heat jump $\Delta C/\Delta C_o$ is related to the reduced critical temperature T_c/T_{co} (ΔC_o and T_{co} are ΔC and T_c of the matrix) by the BCS law of corresponding states $\Delta C/\Delta C_o = T_c/T_{co}$. This correlates with the nearly exponential T_c vs. n curve which is characteristic of such weakly magnetic systems. For the (La, Gd)Al_2 system the Abrikosov-Gor'kov (AG) expression for the reduced specific heat jump as a function of the reduced critical temperature is followed very closely, in agreement with the AG behavior of the T_c vs. n curve. For the superconducting-Kondo system (La, Ce)Al_2 there is a very strong depression of the specific heat jump with decreasing T_c, much faster than predicted by either AG or BCS. This is

related to the recently reported re-entrant T_c vs. n curve, a striking deviation from AG behavior.

The normal state specific heat of all three systems is strongly affected by the impurities. A very large enhancement of the electronic specific heat coefficient γ is observed for the ThU system with $d\gamma/dn = 2.7$ mj/mole °K^2 at. % U at low U concentrations. In the (La, Ce)Al_2 alloys, a Kondo effect occurs in the impurity contribution to the specific heat which varies as (-ln T) between 0.5 and ~ 2.5 °K and presumably exhibits a peak near the Kondo temperature $T_K \sim 0.1$ °K. This exchange scattering anomaly is not visibly affected by an externally applied magnetic field below ~ 1.7 kgauss. In contrast to the (La, Ce)Al_2 system, the (La, Gd)Al_2 heat capacity shows an upturn at low temperatures which is strongly dependent upon external magnetic field. In low fields, it varies as (-ln T) between 0.5 and ~ 3 °K. Surprisingly, both the (La, Ce)Al_2 and (La, Gd)Al_2 systems show a very strong enhancement of γ with $\Delta\gamma = 0.37$ joule/mole Ce °K^2 and $\Delta\gamma = 0.57$ joule/mole Gd °K^2 respectively. Large impurity effects are also observed for both systems in the superconducting state down to temperatures far below T_c.

The experiments were made in He^3 semi-adiabatic calorimeters of varying simple design. Their main features are presented and discussed in some detail.

I. SPECIFIC HEATS OF SUPERCONDUCTORS WITH MAGNETIC IMPURITIES

A. INTRODUCTION

This thesis reports a study of the effect of different magnetic impurities on the superconducting and normal state heat capacities of certain nonmagnetic metals. Experiments and theories have shown that the superconducting ground state is modified by the interactions that determine the magnetic behavior of impurities in metals. We have chosen three matrix-impurity systems in which previous experiments on normal and superconducting properties have suggested that different scattering processes are responsible for the magnetic behavior of the impurities. The nearly nonmagnetic spin fluctuation limit is exemplified by the ThU system; the magnetic limit with positive conduction electron-impurity spin exchange coupling by the (La, Gd)Al_2 system; and the magnetic limit with negative exchange coupling (and in turn the Kondo effect) by the (La, Ce)Al_2 system. The aim of this work is to show that these various magnetic behaviors are also differentiable calorimetrically. We give below a brief description of some aspects of magnetism in dilute alloys, in particular in relation to superconductivity, which forms a background for understanding the motivation and interpretation of the specific heat experiments discussed in this thesis.

The first successful theoretical approaches to the problem of dilute alloys were made by Friedel[1] and somewhat later by Anderson.[2] The main achievement of their early work was the introduction of the concept of a virtual bound state and the establishment of a criterion for when a impurity is expected to carry a magnetic moment in a metallic host. In terms of the Friedel-Anderson model, the magnetic behavior of a single impurity in a metallic host is determined by two competing mechanisms: The intra-atomic Coulomb repulsion U between electrons with opposite spin direction in the outermost partially filled localized electron shell, and the mixing interaction V_{sl} between the free electron states (denoted by s) and the localized orbital (denoted by l). The width of the virtual bound state localized at the impurity site is given by $\Delta = \pi \langle V_{sl}^2 \rangle N(E_F)$, where $N(E_F)$ is the host density of states at the Fermi level. Due to the Coulomb splitting of the spin-up and spin-down states, a magnetic moment of $1\,\mu_B$ (for a singly occupied, nondegenerate orbital state) is localized at the impurity when one of these states lies below the Fermi level. The Coulomb splitting is self-consistently weakened by broadening of the virtual bound state due to the mixing interaction V_{sl}. For large hybridization (large Δ) the magnetic state collapses into a nonmagnetic ground state with the spin-up and spin-down local states degenerate in energy. The model predicts a sharp boundary between magnetism ($\pi\Delta/U < 1$) and nonmagnetism ($\pi\Delta/U > 1$),

known as the Hartree-Fock (hereafter HF) instability.

However, it was soon realized that the Friedel-Anderson model overestimates the tendency towards magnetism and that a much more smooth transition occurs between the two regimes. Further extensions of the model have introduced the concept of "localized spin fluctuations" (hereafter LSF) as an attempt to describe this smooth magnetic-nonmagnetic transition in terms of a characteristic frequency of a time dependent local magnetization. As calculated by Rivier and Zuckerman[3]

$$\tau_{sf}^{-1} = \frac{1 - U N_1(E_F)}{\pi N_1(E_F)} \qquad (1)$$

where $N_1(E_F)$ is the density of localized states at the Fermi level. This quantity becomes unphysical at the HF instability $U N_1(E_F) = 1$,* but now the static, zero temperature Friedel-Anderson picture of the magnetic moment has been transformed into a dynamical model in which the impurity approaches the magnetic regime as the local magnetization is longer lived. The LSF picture has provided a useful way of interpreting the physical properties of dilute alloys in the non-magnetic HF limit ($UN_1(E_F) < 1$), and we shall come back to this later when discussing the ThU system.

Beyond the HF divergence (in the magnetic limit), another model is useful in describing our magnetic systems. In this model,

*No predictions beyond the HF instability are available from the LSF model.

a localized spin $\underset{\sim}{S}$ is assumed to exist at the impurity site, coupled to the electron spin density $\underset{\sim}{s}$ at the impurity site via the Hamiltonian

$$H = -2 J_{sl} \underset{\sim}{s} \cdot \underset{\sim}{S} \tag{2}$$

where J_{sl} is the exchange interaction parameter. Using this interaction for the case of an antiferromagnetic coupling parameter ($J_{sl} < 0$), Kondo[4] was able to explain the resistivity minimum phenomenon which had been observed in many dilute alloys of transition metal impurities in noble metal hosts. His calculation of the scattering cross section in the second Born approximation for $J_{sl} < 0$ shows a logarithmic divergence which appears in the magnetic contribution $\Delta\rho$ to the resistivity; i.e.,

$$\Delta\rho = n\,\rho_m [1 + 4 J_{sl} N(E_F) \ln (T/T_F)] \tag{3}$$

Here n is the magnetic impurity concentration and ρ_m is the spin dependent part of the resistivity in the first Born approximation. Expression (3) is only valid for temperatures $T > T_K$, where $T_K \sim T_F \exp [1/J_{sl} N(E_F)]$; T_K is known as the Kondo temperature and T_F is the Fermi temperature. Further extensions of the theory to low temperatures have removed the divergence at T_K, and some have suggested the existence of a "spin compensated state"[5] below T_K of nonmagnetic nature, and manifested, for example, as a saturation of $\Delta\rho$ for $T \ll T_K$. However, the theoretical situation is not completely clear in the nonmagnetic limit.[6] Recent

experiments on the heat capacity of CuCr alloys ($T_K = 2.11°K$)[7] have shown that the most recent extension of the s-l model to low temperatures seems to give the correct answer down to $T \sim 0.1\ T_K$, but there are departures which become more significant as the temperature is decreased below this value.

We have remarked that the LSF and s-l pictures of the single impurity problem have complementary regions in which they are invalid. One is confronted with the following question: Is the LSF picture the low temperature limit of the s-l model and conversely? This fundamental question is not answered yet, but there is some theoretical evidence for the equivalence of both models[8] and some experiments where it has been shown that by changing pressure[9] or alloying,[10] it is possible to go smoothly from the magnetic to the nonmagnetic regime. Therefore, to characterize the magnetic behavior of dilute alloys we shall use a phenomenological parameter T_o. For those systems where the Kondo picture is a good description, we will regard T_o as T_K; if not, we will relate T_o to the LSF model in the nonmagnetic limit.

In going from high temperatures through T_o, the entropy per impurity atom is expected to be reduced by the degeneracy entropy

$$\Delta S = k_B \ln (2S + 1) \tag{4}$$

if the impurity is nonmagnetic at low temperature. As a direct

consequence, the heat capacity per impurity atom is expected to go through a maximum at temperatures of the order of T_o and the area below such a maximum should be a measure of ΔS as expressed by Eq. (4). This phenomenon has already been observed in CuCr[7] alloys. Recent experiments on the (La, Ce)Al_2 [11] system have revealed a minimum in the resistivity with $\Delta\rho$ linear in ln T and a low temperature departure from a Curie-Weiss law which have suggested that this system is magnetic at low temperatures with $J_{sl} < 0$. We therefore made heat capacity measurements to search for the exchange scattering anomaly in the normal state. However, the observation of this truly single impurity effect is fairly difficult due to the extended range of the anomaly and the problems involved in the separation of the impurity contribution from the total heat capacity. High impurity concentrations which would make the effect more visible are undesirable, since, if the average distance between impurity atoms decreases, new contributions due to the correlations between impurities become more important. We consider briefly the origin of interactions between impurities in order to emphasize differences in the contributions to the heat capacity due to correlation effects as contrasted to the "true" one impurity effect.

Effects Due to Interactions between Impurities

The onset of magnetic order can be visualized if we note that each impurity, via interaction (2), induces an oscillatory spin polarization in the electron gas which depends on distance r as[12]

$$(\rho\uparrow - \rho\downarrow)(r) = J_{sl} S^2 \frac{\cos(2 k_F r)}{(k_F r)^3}; \quad k_F >> 1 \tag{5}$$

where k_F is the Fermi momentum of the conduction electrons. It has been shown that when another impurity is within the range of this perturbation, the electrons interact again with this impurity spin via Hamiltonian (2). As a result, an effective coupling, known as the RKKY[13] interaction, appears between pairs of impurity spins.

Several calculations, performed in the mean field approximation[14,15,16] have shown that the RKKY magnetic contribution to the heat capacity has a broad maximum at a temperature T_M which more recent calculations have shown to depend linearly on impurity concentration.[17] Heat capacity experiments on CuMn,[18] AuFe,[19] YGd,[17] and $(La, Gd)_3Al$ alloys[20] have shown the presence of the ordering maximum at T_M and have confirmed its linear concentration dependence. Recent experiments on PtCo[21] alloys in an extended range of compositions and temperatures have shown a concentration independent maximum in the dilute limit and a strong shift in this maximum to higher temperatures when the concentration is increased above 0.3 atomic percent Co.

Superconductivity and Magnetic Impurities

The superconducting critical temperature of metals has been shown earlier to be strongly depressed by small amounts of magnetic impurities.[22,23] Somewhat later it was realized that the detailed dependence of T_c on impurity concentration gives valuable information about the magnetic nature of the impurities. For the three magnetic impurity regimes considered here, three distinct types of T_c vs. n curves, discussed below, have been established.

When dissolved in $LaAl_2$, Gd impurities are known to retain their free-ion Hund's rule ground state configuration; i.e., a well-defined moment of $7\,\mu_B$ is localized at the impurity site.[24] This case is appropriate to the theory of Abrikosov and Gor'kov (AG)[25] who have calculated the influence of Hamiltonian (2) on the BCS superconducting ground state. Their theory includes the following assumptions: 1) The impurity spins are non-interacting and randomly distributed; and 2) the exchange scattering may be adequately represented in the first Born approximation (to order J_{sl}^2).

According to the AG calculation, the superconducting critical temperature is depressed as a universal function of impurity concentration n given by

$$\ln\left(\frac{T_c}{T_{co}}\right) = \psi\left(\frac{1}{2}\right) - \psi\left(\frac{1}{2} + 0.140\ \frac{T_{co}}{T_c}\ \frac{n}{n_{cr}}\right) \qquad (6)$$

where T_{co} is the transition temperature of the host, ψ is the digamma function and n_{cr} is an adjustable parameter which gives the critical concentration at which superconductivity is completely suppressed ($T_c = 0$). Expression (6) may also be generalized to other pair breaking situations by replacing n/n_{cr} by α/α_{cr} where α is the pairbreaking parameter and α_{cr} is the value of α at which $T_c = 0$. The generalized form of expression (6) can then be written

$$\ln\left(\frac{T_c}{T_{co}}\right) = \psi\left(\frac{1}{2}\right) - \psi\left(\frac{1}{2} + 0.140\ \frac{T_{co}}{T_c}\ \frac{\alpha}{\alpha_{cr}}\right) \qquad (7)$$

The AG prediction for T_c vs. n is shown in Fig. 1(a) with the data of the $(\underline{La}, Gd)Al_2$ [26] system. In this instance the agreement between experiment and theory is excellent. Similar results have been found in the $\underline{Th}Gd$ system, [27] and more recently in the $(\underline{La}, Gd)_3Al$ [20] system. However, it should be noted that strong departures from the AG behavior due to magnetic ordering have been reported in the related systems $\underline{La}Gd$ [22] and $(\underline{La}, Gd)_3In$. [23] In these systems the magnetic ordering temperature depends linearly on Gd concentration and intersects the T_c vs. n plot at a relatively high value of T_c/T_{co}. In the $(\underline{La}, Gd)Al_2$ system, the susceptibility shows a Curie-Weiss temperature dependence [24] and the Curie-Weiss temperature θ decreases rapidly with decreasing concentration. For n = 0.83 a/o Gd (n/n_{cr} = 1.41), θ = 0.07°K, which is much lower than the low temperature limit of the present experiments. Therefore one would not expect

ordering effects in the specific heat data on $(La, Gd)Al_2$ alloys reported in this thesis.

The interaction (2) breaks time reversal invariance. As a consequence, the lifetime of the "Cooper pairs" in a superconductor with magnetic impurities is no longer infinite. The inverse of the lifetime (or pair breaking parameter α) is given in the AG theory by the expression

$$\alpha(n) = n\, N(E_F)\, J_{sl}^2\, S(S+1) \tag{8}$$

Here $\alpha(n)$, calculated in the first Born approximation, depends linearly on concentration, but it should be noted, is independent of temperature.

A different situation occurs for $J_{sl} < 0$; in this case the scattering cross section has to be calculated to higher order than J_{sl}^2 which leads to the Kondo effect. The introduction of the Kondo effect into the A. G. theory[28, 29] can be described in terms of a pair breaking parameter, now dependent on temperature as well as concentration and given, according to Müller-Hartmann and Zittartz (MHZ),[28] by

$$\alpha(n,\ T/T_o) = \frac{n}{2\pi N(E_F)} \frac{\pi^2 S(S+1)}{\ln^2(T/T_o) + \pi^2 S(S+1)} \tag{9}$$

This expression for the pairbreaking parameter has a maximum at

$T/T_o = 1$ and when replaced in the AG expression (7) for the critical temperature predicts a variety of behaviors according to the ratio T_o/T_{co} and the value of S. For the strong magnetic limit ($T_o/T_{co} \ll 1$), a second transition back into the normal state is predicted by simultaneously solving expressions (7) and (9).* Further experiments on (La, Ce)Al_2 [30, 31] alloys have confirmed these predictions in a narrow range of compositions as shown in Fig. 1(b). Assuming $S = 1/2$, the fitting to the theory gives $T_o \cong 0.12°K$.

On the other hand, the temperature dependent pair breaking picture seems to fail in the nonmagnetic limit $T_o \gg T_{co}$ as suggested previously[32] and confirmed in this work by specific heat measurements on ThU alloys. In the ThU system, measurements of the normal state electrical resistivity, thermoelectric power, and magnetic susceptibility[33] have indicated a characteristic temperature $T_o \sim 100°K$. The T_c vs. n curve (Fig. 1(c)) shows an almost exponential behavior, similar to that observed in the AlCr[34] and AlMn[35] systems whose normal state physical properties have been interpreted in the framework of the LSF model. Furthermore, the T_c vs. n curves of these systems, and the ThU system as well, are described very well by a modified exponential relation recently proposed by

---

*A third transition temperature at which the sample again enters the superconducting state is also predicted by expressions (7) and (9) in the limit $T_o/T_{co} \ll 1$, but it has not been observed experimentally.

Kaiser[36] where the pair weakening effect on T_c is due to the nonmagnetic resonant states associated with the impurities. These physical properties suggest that there is a localized magnetization at the U sites which fluctuates in time with a characteristic frequency

$$\tau_{sf}^{-1} = \frac{k_B}{h} T_o \tag{10}$$

and that at temperatures much lower than T_o, the ThU system is essentially nonmagnetic. However the low value of T_o places its magnetic behavior relatively close to the HF instability and recently some attempts have been made to fit the ThU T_c vs. n results to the low temperature nonmagnetic limit of the Kondo-pair breaking picture.[28,29] We have measured the heat capacity of this system since, as discussed below, these measurements are particularly sensitive to the magnetic character of the impurities.

The Specific Heat Jump at the Superconducting Transition Temperature

The specific heat jump ΔC at T_c is another powerful method for distinguishing the magnetic behavior of the impurities. For BCS superconductors the relationship between ΔC and T_c is given by[37]

$$\Delta C = \beta \gamma T_c \tag{11}$$

where β is a universal constant of the order of 1.5 which has been verified for many superconductors, and γ is the electronic specific

heat coefficient. When the critical temperature of a superconductor is changed by adding nonmagnetic solutes, the specific heat jump should change in accordance with this relationship. If the density of itinerant states at the Fermi level remains unchanged by the addition of nonmagnetic impurities (certainly a valid assumption in the dilute impurity limit), the BCS Law of Corresponding States can then be expressed as

$$\Delta C/\Delta C_o = T_c/T_{co} \tag{12}$$

where ΔC and T_c are the specific heat jump and critical temperature for an alloy of concentration n, while ΔC_o and T_{co} are the corresponding quantities for the matrix into which the impurities are dissolved (Fig. 2).

However, in the case of magnetic impurities, AG showed that the energy gap decreases faster than T_c with increasing impurity concentration. The resultant marked deviation of $\Delta C/\Delta C_o$ from the BCS Law of Corresponding States predicted by AG for magnetic impurities is also shown in Fig. 2.[38] Since this deviation from BCS behavior is a direct consequence of the pair breaking character of Hamiltonian (2), we expect even more pronounced effects in the case of temperature dependent exchange scattering.

FIGURE 1

Superconducting transition temperature versus impurity concentration for:

(a) (La, Ce)Al_2 (from Ref. 31)

(b) (La, Gd)Al_2 (from Ref. 26)

(c) ThU (from Ref. 33)

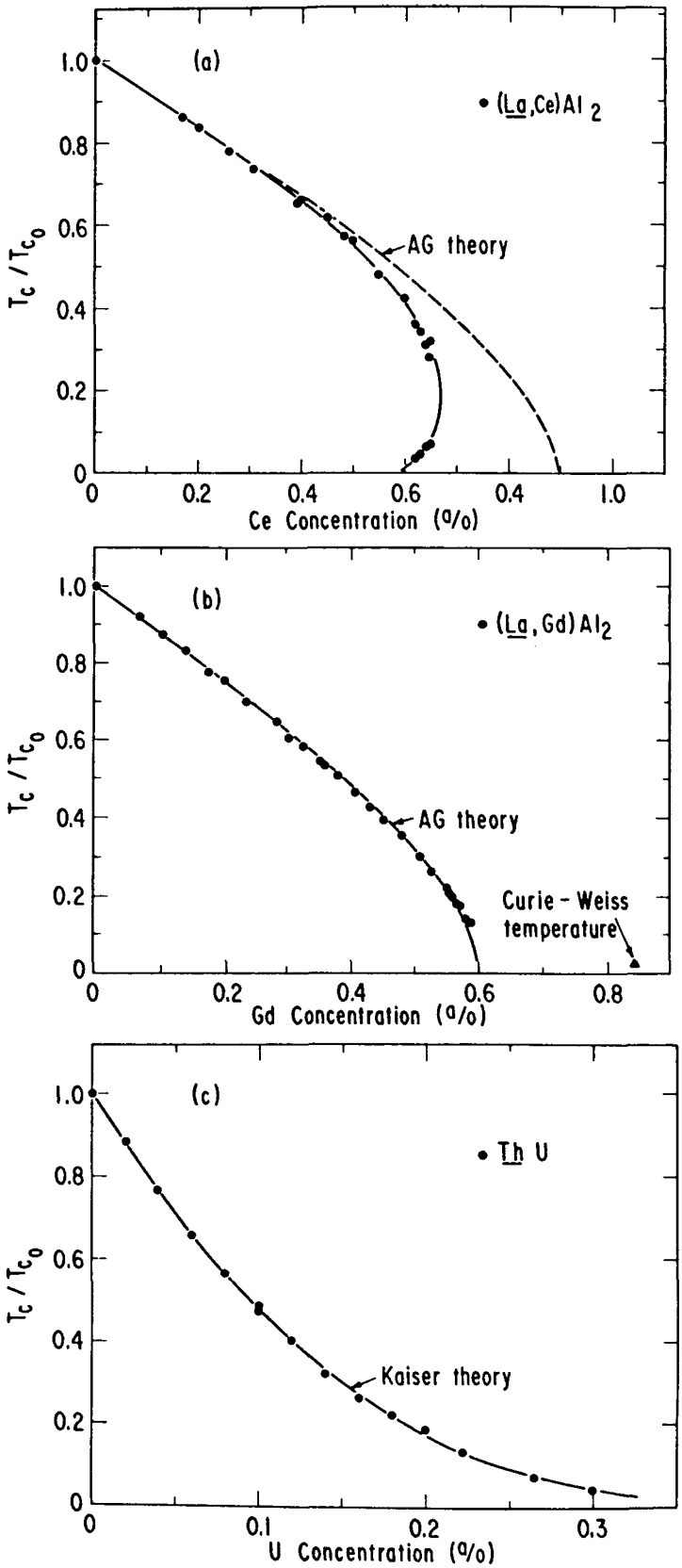
(a)
• (La,Ce)Al 2
AG theory
T_c / T_{c_0}
Ce Concentration (a/o)
(b)
• (La, Gd) Al2
AG theory
Curie - Weiss temperature
Gd Concentration (a/o)
(c)
• Th U
Kaiser theory
U Concentration (a/o)

FIGURE 2

Reduced specific heat jump $\Delta C/\Delta C_o$ vs. reduced critical temperature T_c/T_{co}.

-----BSC Law of Corresponding States

———AG theory (from Ref. 38)

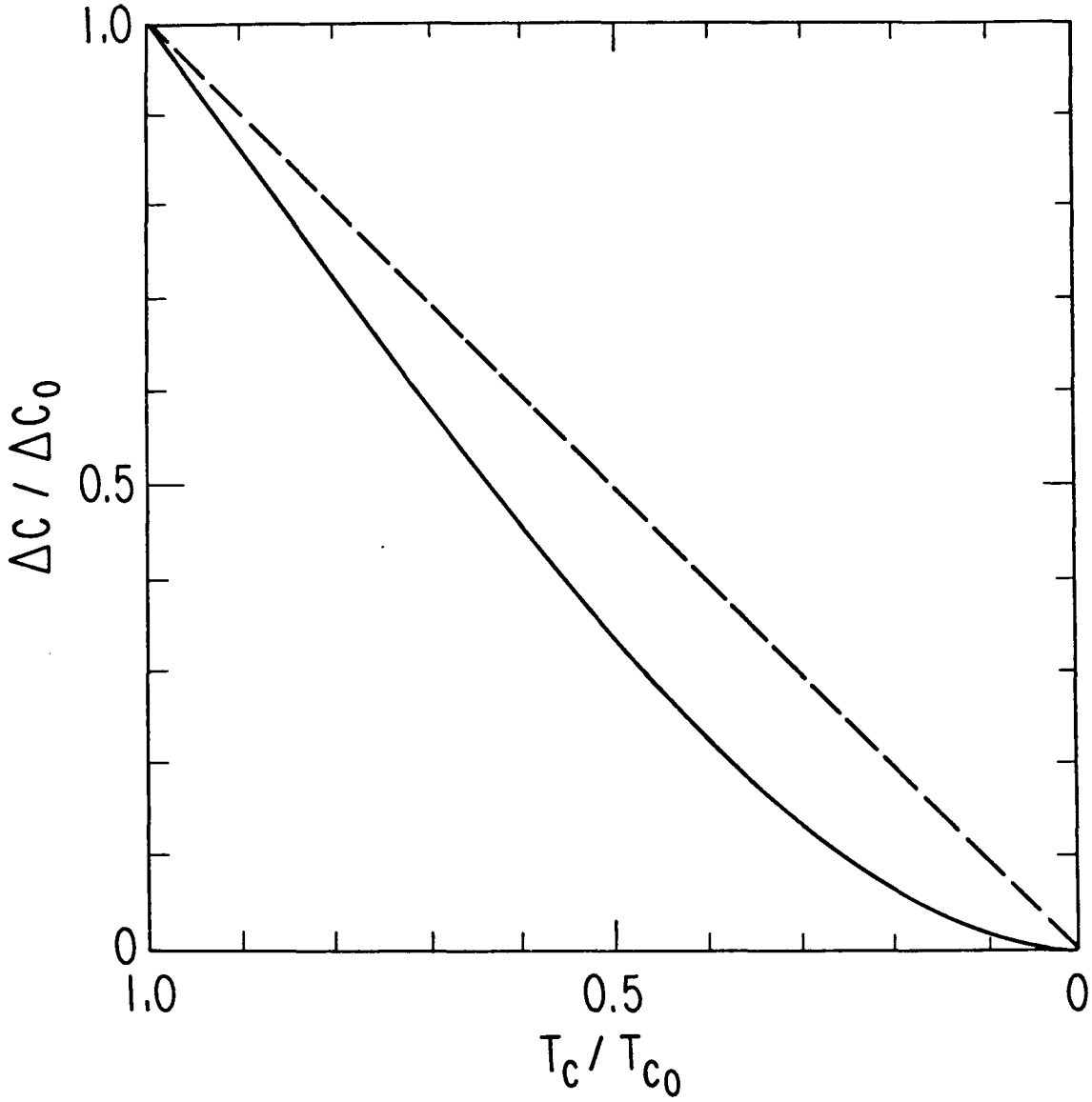
1.0
0.5
0
1.0
0.5
0
ΔC / ΔC0
Tc / Tc0

B. RESULTS

1. The ThU System: A Superconductor with Localized Spin Fluctuations

Sample Preparation

Samples were prepared from 99.95% pure Alfa Inorganics-Ventron Thorium and high purity Los Alamos uranium by arc melting in an argon atmosphere. The samples were remelted several times to increase homogeneity. Several facts indicated a homogeneous distribution of impurities in the samples. The transition widths, measured by an a.c. mutual inductance technique, were never greater than 35 m°K in spite of the large size of the samples (11 to 19 gms.); the bulk calorimetric temperatures agreed within 3% with the a.c. critical temperatures, and the calorimetric transitions were sharply peaked.

Two sets of experiments were made: First, pure thorium and dilute samples of 0.075 and 0.134 at.% U were measured[40, 41]. The weight of these samples did not exceed 11 gms. Later, a more precise and more extensive set of experiments was made on bigger samples (~18 gms) of compositions 0.065, 0.110, 0.50, 1.00, and 2.10 at.% U.[42, 43] Finally, a new, larger sample of pure thorium was also measured.

Specific Heat Results

For all the samples investigated, between 60 and 85 experimental points were fitted to the usual relation

$$C_v = \gamma T + \beta T^3$$

between 1.0 and 5.0°K in the case of the alloys, and between 1.4 and 4.2°K in the case of the second thorium sample. An illustrative C_v/T vs. T^2 plot is shown in Fig. 3 for several of the samples investigated. The values obtained for the normal state parameters γ and the Debye temperature θ_D are given in Table I. Previous results for pure thorium are also included.

The values for the remeasured Th sample, considered more reliable than the less sensitive preliminary values, are in reasonable agreement with the heat capacity data of Gordon et al.[44] and the critical field data of Decker and Finnemore.[45] The most significant result of the measurements in the normal state is the very large rate at which γ increases with U concentration: $d\gamma/dn = 2.7$ mj/mole°K^2 at.% U at low concentrations and becomes somewhat less at higher concentrations (Fig. 3, inset), presumably due to interactions between impurities. Similar saturation effects have been observed in AuV.[46] The θ_D values in Table I indicate that there is no systematic change in θ_D due to alloying.

Measurements were also extended into the superconducting state for pure Th and the three most dilute ThU alloys.* The

*Measurements become more difficult at the lowest temperature because of the radioactivity of the samples which give a heat input of about 150 erg/min at 0.7°K (determined from the recorded self heating rates for the largest samples).

electronic specific heat below 2°K is shown in Fig. 4. The value $\Delta C_o / \gamma T_{co} = 1.46 \pm 0.03$ for the Th matrix agrees well with the theoretical BCS value of 1.43[37] and previously reported values.[44,45] Furthermore, the specific heat jumps for the alloys followed closely the BCS Law of Corresponding States as illustrated in Fig. 13.

TABLE I

Specific Heat Data for ThU Alloys

n at.% U	γ mj / mole°K^2	θ_D °K	$\Delta\gamma/n$ mj /mole°K^2 at.% U	T_c °K	ΔC mj / mole°K
0*	4.08±0.03	160.4±0.5			8.6 ± 0.2
0	4.28±0.05	164.1±0.5		1.360±0.005	8.50± 0.2
0.065	4.45±0.03	161.9±0.3	2.6	0.860±0.005	5.3 ± 0.3
0.075*	4.45±0.08	161.3±1.0	2.3	0.785	5.3 ± 0.5
0.110	4.58±0.03	161.7±0.3	2.7	0.550±0.005	3.3 ± 0.3
0.134*	4.72±0.04	163.7±0.7	3.3		
0.50	5.28±0.05	162.1±0.5	2.0		
1.00	5.93±0.04	161.9±0.4	1.67		
2.10	7.70±0.06	161.4±0.4	1.62		
0**	4.31±0.05	163 ± 0.7		1.374	8.4

*First set of samples.[40]

**From Ref. 44.

FIGURE 3

C/T vs. T^2 in the normal state for several ThU alloys.

Inset: Electronic specific heat coefficient as a function of U impurity concentration.

△ - First set of samples

● - Second set of samples

□ - From Reference 44.

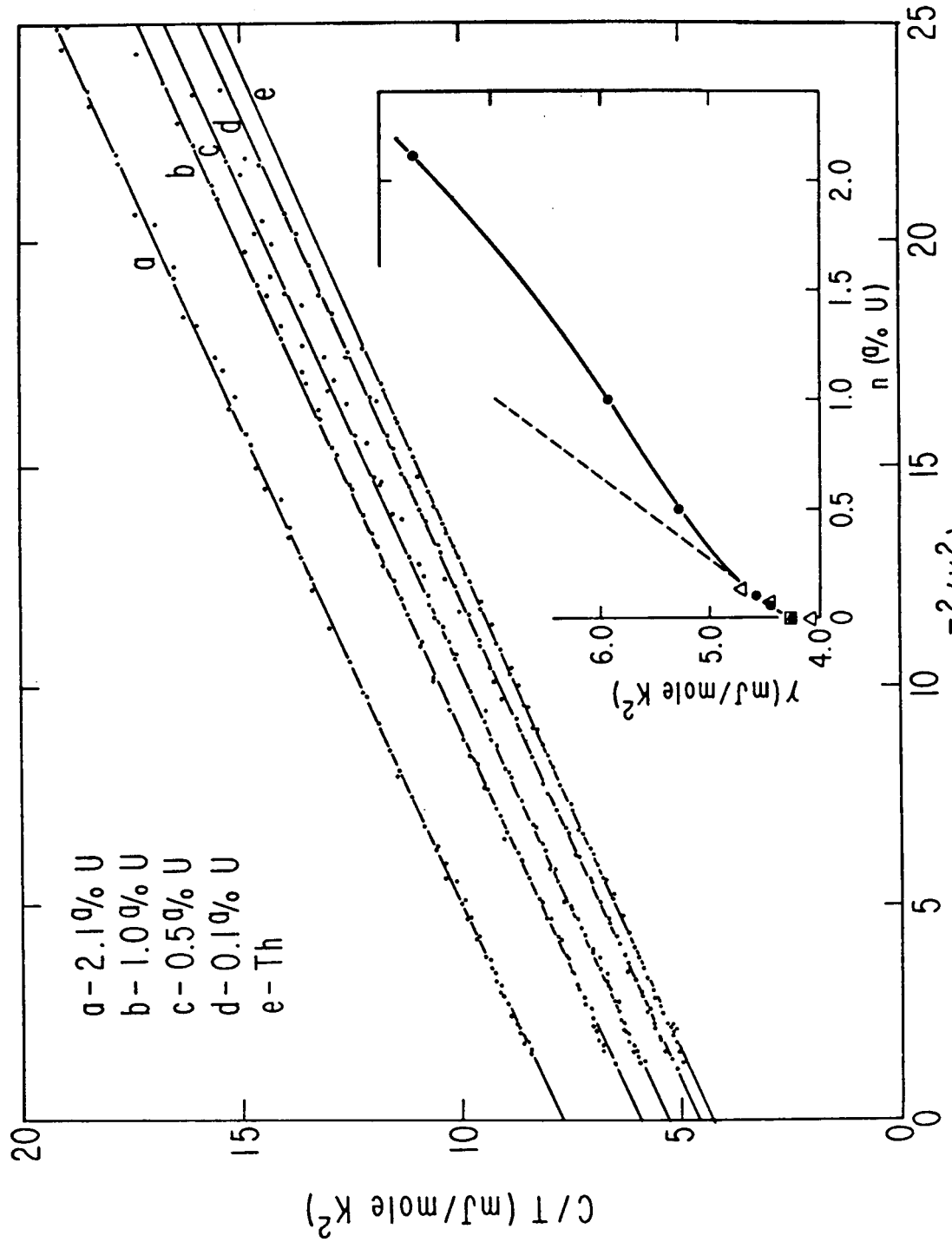
C / T (mJ/mole K²)
T² (K²)
a - 2.1% U
b - 1.0% U
c - 0.5% U
d - 0.1% U
e - Th
a
b
c
d
e
γ (mJ/mole K²)
n (% U)

FIGURE 4

Electronic specific heat below 2°K for pure Th and two ThU alloys.

▲ - Normal state specific heat of pure Th. Below T_c, a magnetic field of about 800 gauss was used to quench superconductivity.

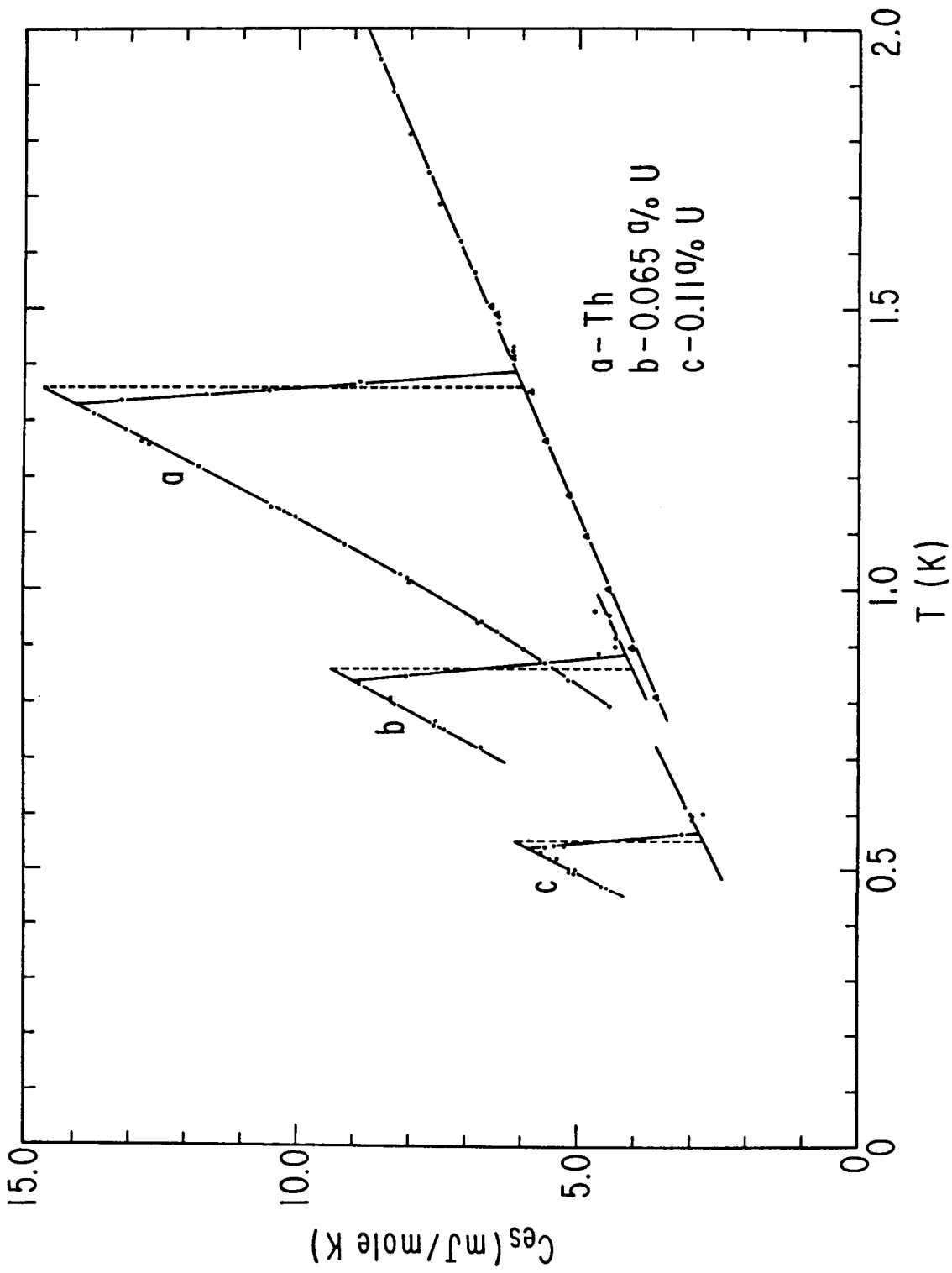
15.0
10.0
5.0
0
0
0.5
1.0
1.5
2.0
T (K)
C_{es} (mJ/mole K)
a
b
c
a-Th
b-0.065 a% U
c-0.11a% U

2. The (La, Ce)Al_2 System: A Kondo Superconductor

Sample Preparation

The samples were prepared in two steps. First, LaCe alloys were made by arc-melting appropriate amounts of La and Ce (both obtained from Johnson-Matthey; nominal purity for La, 99.99%,[47] and for Ce, 99.99%) together in an argon atmosphere. The calculated weight of 99.999% pure Al (Semi-Alloys, Inc.) was added to each LaCe alloy to form the corresponding (La, Ce)Al_2 compound.[48] During fabrication the alloys were remelted many times to achieve a homogeneous distribution of the impurities. The arc-melted ingots, wrapped successively in foils of Ta, Zr, and Ta, were then annealed for 16 hours at 800°C in a helium atmosphere. This procedure has previously been found to sharpen considerably the superconducting transitions.[49]

Each sample weighted between 5 and 6 gms and had a heat capacity at 1°K equivalent to that of ~25 gms of pure copper at the same temperature. The nominal compositions (0.185, 0.401, and 0.527 at.% Ce substitution in La) agreed closely with those deduced from the calorimetric critical temperatures and the T_c vs. Ce concentration curve previously obtained[49] from the inductively measured T_c's of much smaller samples. The widths of the calorimetric transitions (Table II) indicated a fairly homogeneous distribution of the impurities; however, the transitions became wider with increasing

the Ce concentration. The critical temperatures were also measured with an a.c. technique but superconducting surface effects were found to give critical temperatures up to 3% higher than the bulk transitions measured by specific heat. The single peaked, relatively sharp calorimetric superconducting transitions reflected the excellent quality of the samples and correlated with x-ray and microprobe analysis made on smaller samples, which indicated the presence of a single metallographic phase.[49]

Specific Heat Results

Specific heat measurements were made in both the normal and the superconducting states for all the samples. To quench superconductivity, magnetic fields of 850 and 1700 gauss were applied with a superconducting solenoid. The normal state specific heat was found to be independent of the magnetic field in this range within the precision of the measurements. As the magnetoresistance of the germanium thermometer resulted in calibration shifts of less than 1 m°K/KG at 4.2°K and 0.3 m°K/KG at 0.5°K, no corrections were made to the zero field calibration.

The specific heat C_v vs. temperature T of $LaAl_2$ and the three $(La, Ce)Al_2$ alloys between 0.5 and 4.2°K is shown in Fig. 5.[50] In order to eliminate the lattice specific heat a βT^3 term, corresponding to a Debye temperature θ_D of 376 ± 3°K, has been subtracted from the data. A very strong low temperature anomaly in the

heat capacity which increases with the impurity concentration is clearly visible for normal and superconducting state alike. A first glance at Fig. 5 shows that the specific heat jumps are strongly depressed from that of pure $LaAl_2$. In fact, when the reduced specific heat jumps $\Delta C/\Delta C_o$ are plotted as a function of the reduced critical temperature T_c/T_{co}, strong departures from the BCS Law of Corresponding States are observed (Fig. 13).

In Fig. 6, the specific heat in the superconducting state is shown in a semilogarithmic $C_s/\gamma T_c$ vs. T_c/T plot for the $LaAl_2$ matrix and all the alloys measured. The value of $C_s/\gamma T_c$ at $T = T_c$ for $LaAl_2$ is 2.39. The close agreement with the BCS value of 2.43 is consistent with the exponential behavior observed for $T < T_c$. The low temperature departure from the theoretical prediction (Fig. 6) is similar to those observed for the alloys and it is attributed to the presence of Ce impurities in the La starting material.

For the alloys studied here, C_s goes to zero as a function of temperature much more slowly than exponentially. C_s/T vs. T^2 plots show that C_s may be reasonably well represented at low temperatures by the relation

$$C_s = \alpha_s/T^n + \gamma_s T + \beta_s T^3 \qquad (13)$$

where $n \sim 2.8$. Although this decomposition is rather arbitrary, we have nevertheless estimated γ_s values (tabulated in Table II) from

our data below 1.2°K. The γ_s so deduced varies with impurity concentration as

$$\gamma_s/\gamma_N = -0.22 + 2.08\, n \qquad (14)$$

where n, the Ce concentration, is expressed in at.%. This suggests that there may be a critical Ce concentration ($\sim$ 0.1 at.%) below which $\gamma_s = 0$. Expression (14) also implies that $\gamma_s = \gamma_N$ at $\sim$ 0.6 at.% Ce, which is near the concentration (0.67 at.% Ce) of the turning point of the re-entrant T_c vs. n curve (Fig. 1), above which the samples are normal down to 6 m°K. It is tempting to relate the appearance of the $\gamma_s T$ term in the superconducting state with the vanishing of the energy gap as previously done by Culbert and Edelstein[51] with regard to their specific heat study on LaCe alloys in the superconducting state. The α_s/T^n term is due to the presence of Ce impurities whose influence persists even in the superconducting state, indicating that the upturn observed in the normal state is really a intrinsic property of the system and not due to the externally applied magnetic field used to quench the superconductivity. Values of ΔC, T_c and the transition width ΔT_c for $LaAl_2$ and the three $(La, Ce)Al_2$ alloys are collected in Table II.

Marked effects in the specific heat of $(La, Ce)Al_2$ are not restricted to the superconducting state. Those encountered in the normal state take the form of a large enhancement of the normal state electronic specific heat coefficient γ_N, increasing at the rate

(0.37 ± 0.02) joule/mole Ce°K^2, and an exchange scattering anomaly which becomes appreciable below 2.5 °K, varying as $\delta C = a - b \ln T$, with $a = \left(0.54 \begin{smallmatrix}+0.05\\-0.01\end{smallmatrix}\right)$ joule/mole Ce°K and $b = \left(0.58 \begin{smallmatrix}+0.09\\-0.05\end{smallmatrix}\right)$ joule/mole Ce°K $(0.5 < T < 2.5\,°K)$. Both contributions scale with Ce concentration within experimental error* indicating that the observed anomalies are single impurity effects.

The contributions mentioned above become strongly visible in the C_v/T vs. T^2 plots shown in Fig. 7 (again the βT^3 term has been removed). In these plots, an enhancement of the electronic specific heat coefficient γ_N appears as a vertical displacement of the linear part of the curves at the higher temperatures. The upturn at low temperatures appears to be the high temperature portion of an exchange scattering anomaly which should have a maximum near the (La, Ce)Al_2 Kondo temperature ($T_K \sim 0.1\,°K$). Unfortunately, the expected maximum falls in a temperature range below the lower limit of 0.5 °K accessible in the present experiments. To find the form of the anomaly above 0.5 °K, a $\gamma_N T$ term has been subtracted from the specific heat of each alloy where the average value of γ_N has been determined from the data between 2.7 and 4.2 °K. The resultant excess specific heat δC (per mole Ce) due to exchange

---

*The small increase of C_v/T at low temperature observed for the $LaAl_2$ matrix is most likely due to Ce impurities in the La starting material.

TABLE II

Specific Heat Data for (La, Ce)Al_2 Alloys

n	γ_N	$\Delta\gamma/n$		T_c	ΔT_c	ΔC		
at. % Ce	$\frac{mj}{mole \cdot K^2}$	$\frac{mj}{mole \cdot K^2}$	$\frac{1}{at.\% Ce}$	°K	°K	$\frac{mj}{mole \cdot K}$	$C_s/\gamma_N T_c$	γ_s/γ_N
0	9.55 ± 0.05	----		3.305	0.030	43.2 ± 0.5	2.39	---
0.185	10.2 ± 0.05	3.5 ± 0.4		2.810	0.080	29.4 ± 1.0	1.88	0.18
0.401	10.6 ± 0.10	2.6 ± 0.4		2.162	0.135	15.45 ± 1.4	1.75	0.58
0.527	11.5 ± 0.05	3.8 ± 0.1		1.745	0.220	6.15 ± 0.6	1.42	0.90

$\theta_D = 376 \pm 3°K$

FIGURE 5

Specific heat of $LaAl_2$ and three (La, Ce)Al_2 alloys in the normal and superconducting states (the lattice contribution has been removed).

● - H = 0 gauss

■ - $LaAl_2$ H = 1700 gauss;

0.185 a/o Ce H = 1700 gauss;

H = 850 gauss;

0.401 a/o Ce H = 1700 gauss;

0.527 a/o Ce H = 825 gauss.

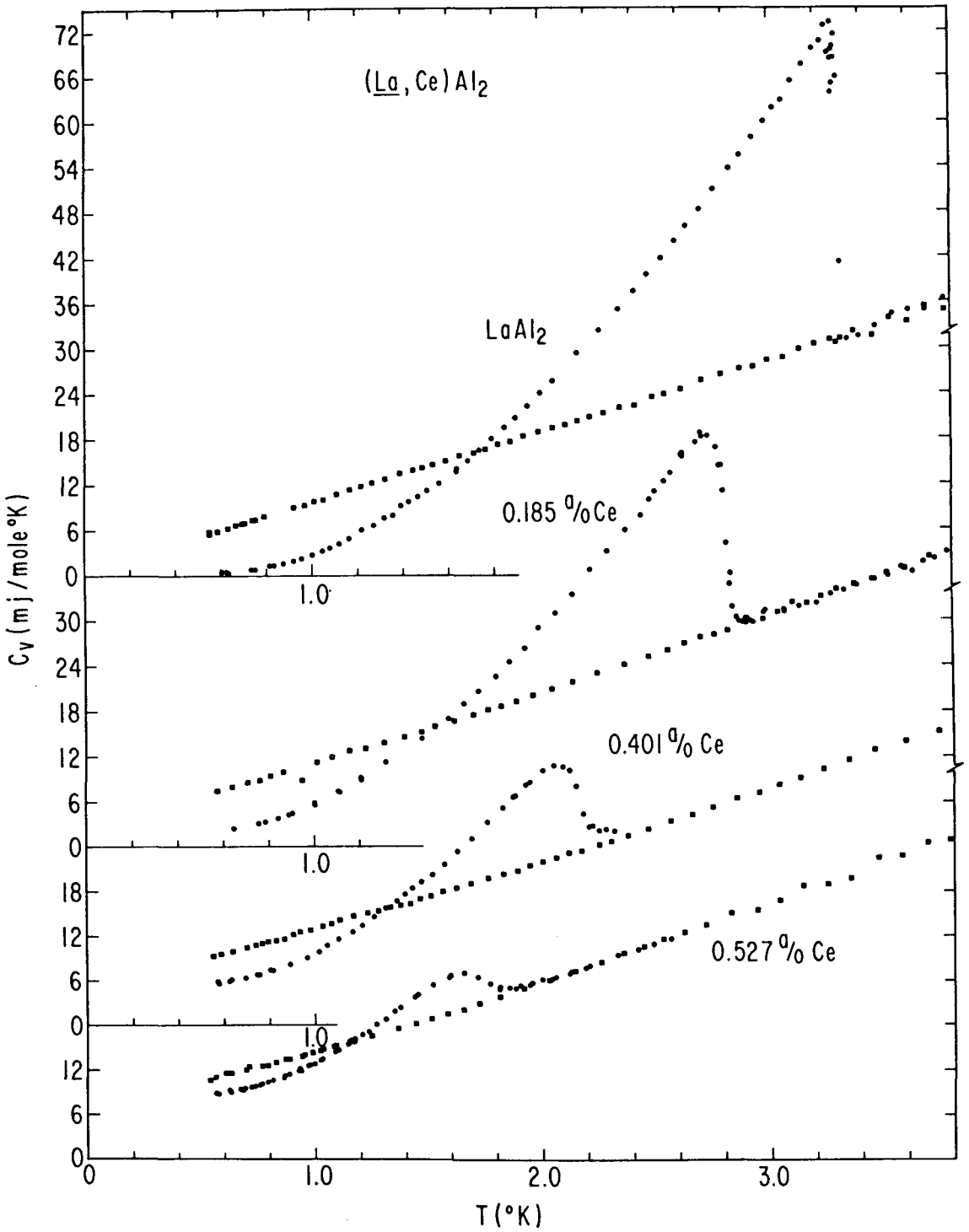
(La, Ce) Al2
LaAl2
0.185 % Ce
0.401 % Ce
0.527 % Ce
Cv (mj/mole °K)
T (°K)
0
1.0
2.0
3.0
72
66
60
54
48
42
36
30
24
18
12
6

FIGURE 6

$C_s/\gamma T_c$ vs. T_c/T in the superconducting state (the lattice contribution has been removed).

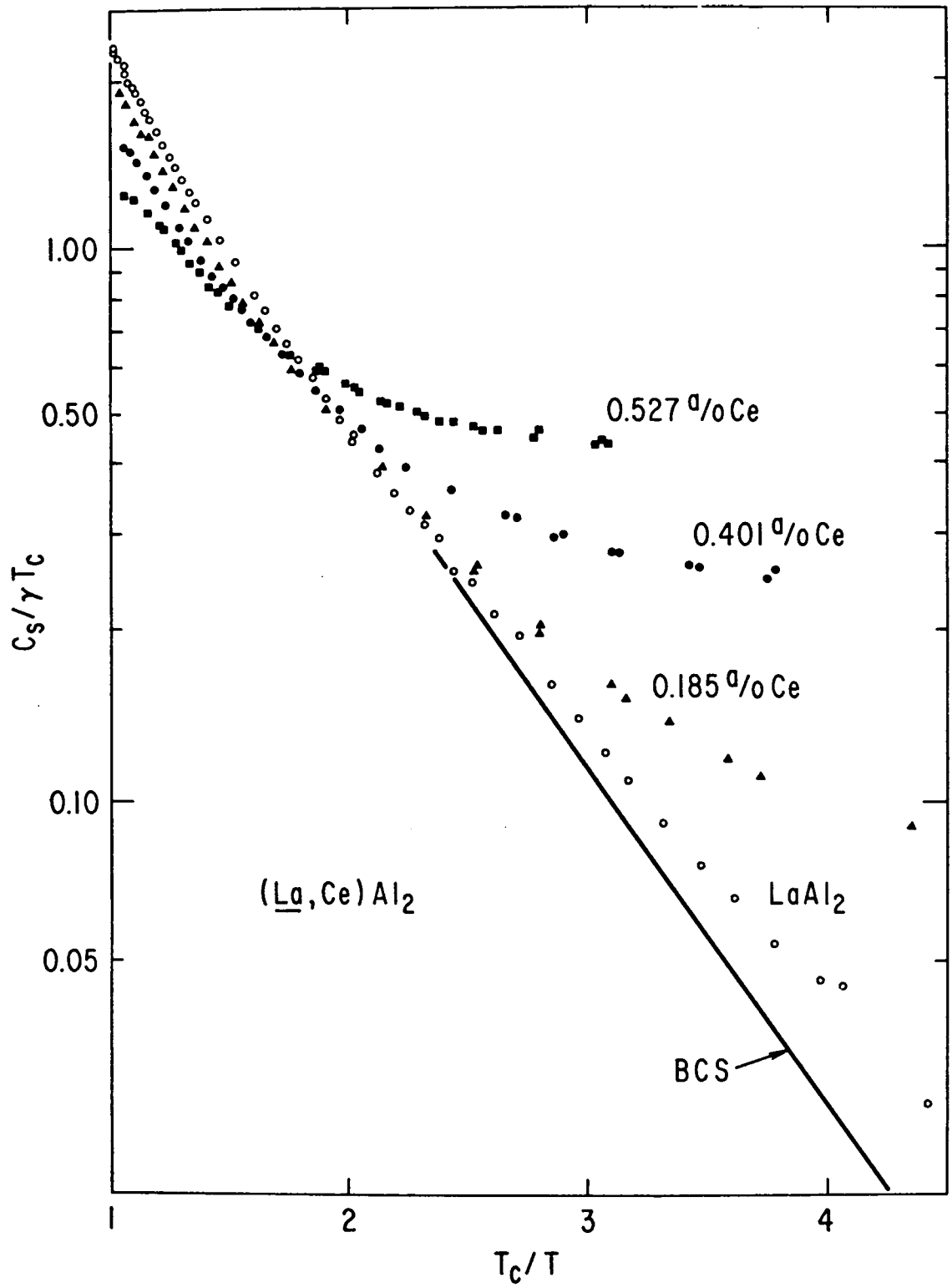
1.00
0.50
0.10
0.05
$C_s/\gamma T_c$
0.527 a/o Ce
0.401 a/o Ce
0.185 a/o Ce
(La, Ce) Al_2
$LaAl_2$
BCS
1
2
3
4
T_c/T

FIGURE 7

C_v/T vs. T^2 in the normal state (the lattice contribution has been removed).

○ - $LaAl_2$

▲ - 0.185 a/o Ce

● - 0.401 a/o Ce

■ - 0.527 a/o Ce

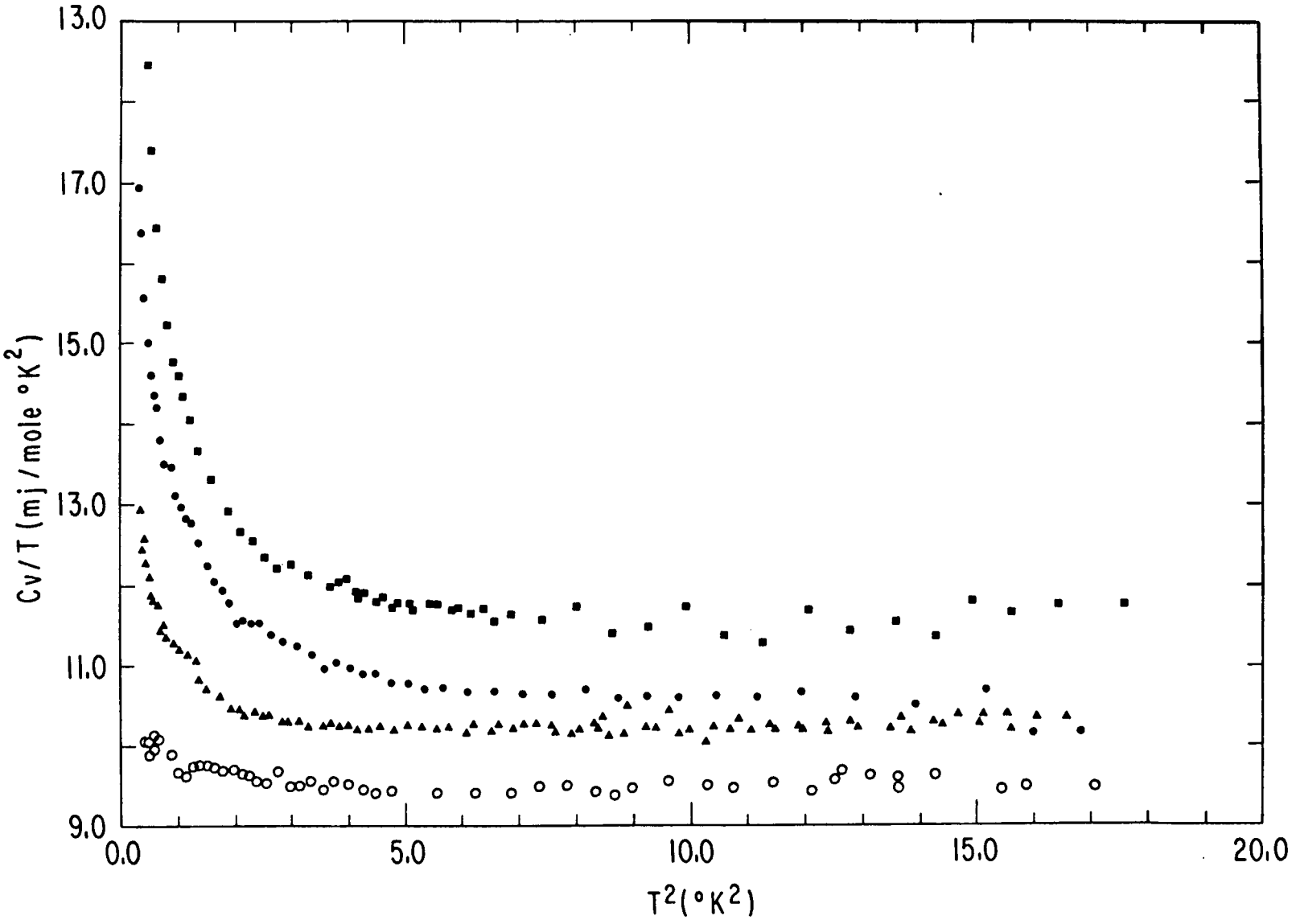
13.0
17.0
15.0
13.0
11.0
9.0
Cv/T (mj/mole °K²)
0.0
5.0
10.0
15.0
20.0
T²(°K²)

FIGURE 8

Excess heat capacity δC due to exchange scattering in the normal state (the linear contribution to the total heat capacity of each alloy has been removed, as well as the βT^3 lattice term).

▲ - 0.185 a/o Ce

● - 0.401 a/o Ce

■ - 0.527 a/o Ce

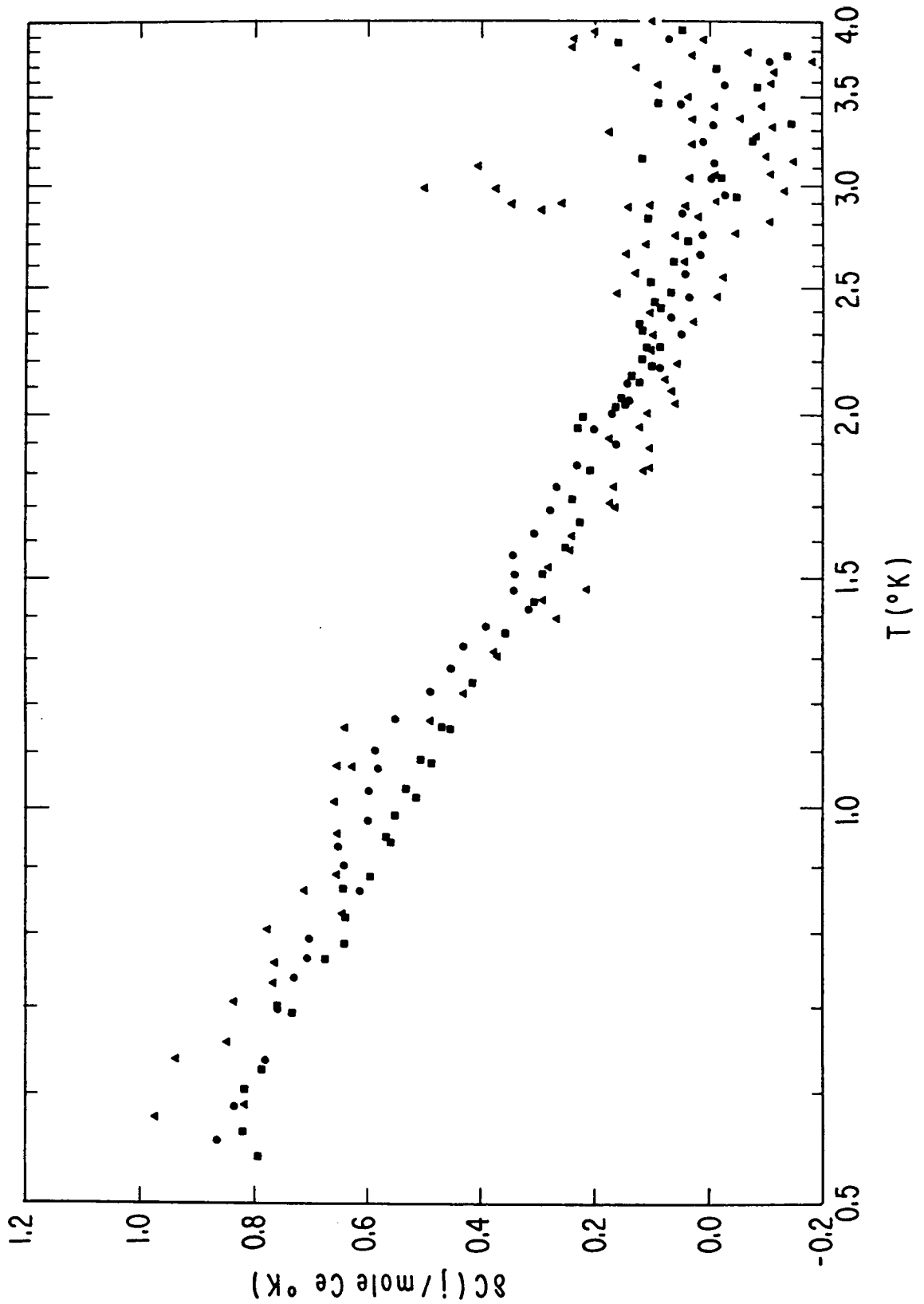
1.2
1.0
0.8
0.6
0.4
0.2
0.0
-0.2
0.5
1.0
1.5
2.0
2.5
3.0
3.5
4.0
T (°K)
δC (j/mole Ce °K)

scattering is plotted vs. ln T in Fig. 8. Within the scatter of the data, δC is proportional to Ce concentration and varies linearly with ln T between 0.5 and $\sim 2.5°K$.

Collected in Table II are the normal state parameters γ_N and $\Delta\gamma_N/n$ where $\Delta\gamma_N = \gamma_N - \gamma_{N_o}$, γ_{N_o} being the electronic specific heat coefficient of the $LaAl_2$ matrix.

3. The (La, Gd)Al_2 System: An Abrikosov-Gor'kov Superconductor

Sample Preparation

The sample preparation procedure was identical to that of the (La, Ce)Al_2 alloys described in section B. 2. Gadolinium (Research Chemicals, 99.9% pure) was used as the impurity instead of cerium.[52] Two samples weighing approximately 6 gms were prepared. The nominal compositions were 0.211 and 0.416 at. % Gd substitution in La. The calorimetric critical temperatures were somewhat lower than those determined previously from a. c. inductance measurements on much smaller, unannealed samples; the calorimetric temperature of the more concentrated sample being lower by about 7%. This reveals the influence of the annealing procedure, similar to that found in the (La, Ce)Al_2 alloys.[53]

Specific Heat Results

Measurements were made in both the normal and superconducting states on the two samples. To quench superconductivity, a

magnetic field of 1700 gauss was applied to the more dilute sample. The normal state measurements on the more concentrated sample were performed in fields of 270, 1700, and 3400 gauss since a strong magnetic field dependence of the specific heat was found.

The specific heat C_v vs. temperature T of the two $(\underline{La}, Gd)Al_2$ alloys in both the normal and superconducting states is shown in Fig. 9.[54] A βT^3 term, corresponding to the same Debye temperature of the $LaAl_2$ and $(\underline{La}, Ce)Al_2$ alloys, has been subtracted from the raw data. The relatively small magnitude of the lattice contribution makes any change in the Debye temperature due to alloying completely unobservable within the precision of the experiments.

The effect of Gd impurities on the superconducting state, as in the case of Ce impurities, is very strong. In Fig. 13, the reduced specific heat jump is plotted as a function of the reduced critical temperature for the two alloys. The experimental data show a remarkable agreement with the AG theory for randomly oriented, uncorrelated magnetic impurities in superconductors. The observed values of the critical temperatures T_c, the specific heat jumps ΔC, and the transition widths ΔT_c, are collected in Table III.

A semilogarithmic plot of $C_s/\gamma_N T_c$ vs. T_c/T for the experimental data below the superconducting critical temperature is shown in Fig. 10. The deviations from the BCS exponential behavior are even stronger than those due to Ce impurities; i.e., the heat capacity

in the superconducting state is much larger for Gd alloys than for Ce alloys (at the same temperature and similar concentrations). These zero field measurements indicate that an exchange scattering anomaly also exists in the Gd alloys and its magnitude is larger than that found in the Ce alloys. However, this anomaly cannot be related to the Kondo effect since J_{sl} is known to be positive for Gd impurities (see section A).

We have plotted in Fig. 10 the theoretical AG predictions for the heat capacity below T_c. The deviations clearly visible at the lowest temperatures are attributed to the onset of ordering effects in the superconducting state. A small field of 270 gauss was enough to destroy the superconducting state in the sample containing 0.416 a/o Gd. After removing the small lattice contribution from the raw data, a C_v/T vs. T^2 plot (see Fig. 11) revealed that the normal state specific heat can be separated into a linear contribution which reflects a strong enhancement of the electronic term of the $LaAl_2$ heat capacity ($\Delta\gamma$ = 0.565 joule/mole Gd°K^2) and a low temperature upturn similar to that observed in the (La, Ce)Al_2 alloys. In addition, measurements on the same sample in fields of 1700 and 3400 gauss revealed a very strong field dependence of the heat capacity below $\sim$ 3.5°K.

The sample containing 0.211 a/o Gd was measured in the normal state only in a magnetic field of 1700 gauss. The coefficient

of the linear term was found to be strongly enhanced ($\Delta\gamma = 0.572$ joule/mole Gd°K^2; again, see Fig. 11) and close to the value obtained for the 0.416 a/o Gd sample. This suggests that the impurity contribution is linear in concentration. However, the strong field dependence observed at low temperatures, even for this dilute sample, obscures the concentration scaling at the lower temperatures measured here. This experimental uncertainty, as yet unresolved, prevented us from making a definitive statement about the concentration dependence of the magnetic contribution.

Further information is obtained from Fig. 12 where the low temperature data have been plotted vs. ln T for the 0.416 a/o Gd sample. Here both the lattice and the electronic contribution to the total heat capacity have been subtracted from the raw data. The low field (270 gauss) behavior shows a linear dependence in (-ln T), remarkably similar to that observed in the ($\underline{La}$, Ce)Al_2 alloys (presented too in Fig. 12 for comparison). The observed anomaly changes with temperature as $\delta C = a - b \ln T$ between 0.5°K and $\sim$ 3°K, where $a = (1.95 \pm 0.02)$ joule/mole Gd°K and $b = (1.74 \pm 0.02)$ joule/mole Gd°K. As the value of the external magnetic field is raised, the heat capacity is seen to increase strongly. The linear dependence in (-ln T) is distorted, and, in the highest field

(3400 gauss), a maximum in the low temperature anomaly is visible in our range of temperatures. The magnetic entropy associated with the excess heat capacity can be estimated in the case of the high field data. If the data are extrapolated linearly to 0°K from the lowest temperature measured here (~ 0.5°K), the entropy per Gd atom associated with the anomaly is $\sim 0.77\ k_B \ln 8$, which is close to the expected value of $k_B \ln 8$. However, further experiments at lower temperature or higher fields are needed before definite conclusions can be drawn.

Collected in Table III are the normal state parameters γ_N and $\Delta\gamma_N/n$ where $\Delta\gamma_N = \gamma_N - \gamma_{N_o}$, γ_{N_o} being the electronic specific heat coefficient of the $LaAl_2$ matrix.

C. CONCLUSIONS

We remark here upon the correspondence we have found between the reduced specific heat jump $\Delta C/\Delta C_o$ vs. the reduced critical temperature T_c/T_{co} plots (see Fig. 13) and the detailed behavior of the superconducting critical temperature T_c vs. impurity concentration n.

The behavior observed for the (La, Gd)Al_2 alloys agrees extremely well with the theoretical prediction of AG as does the previously measured T_c vs. n curve of this system (Fig. 1(b)). The present work gives further support to the idea that the Gd impurities

TABLE III

Specific Heat Data for $(La, Gd)Al_2$ Alloys

n	γ_N	$\Delta\gamma/n$		T_c	ΔT_c	ΔC	
at. % Gd	$\frac{mj}{mole \cdot K^2}$	$\frac{mj}{mole \cdot K^2}$	$\frac{1}{a/o\ Gd}$	°K	°K	$\frac{mj}{mole \cdot K}$	$C_s/\gamma T_c$
0	9.55 ± 0.05			3.305	0.030	43.2 ± 0.05	2.39
0.211	10.75 ± 0.07	5.76 ± 0.5		2.40	0.075	27.4 ± 1.0	2.06
0.416	11.90 ± 0.07	5.67 ± 0.3		1.39	0.120	10.35 ± 0.45	1.92

$\theta_D = 376 \pm 3°K$

FIGURE 9

Heat capacity of (La, Gd)Al_2 alloys in the normal and superconducting states (the βT^3 lattice term has been removed).

● – H = 0 gauss

■ – 0.211 a/o Gd H = 1700 gauss

0.416 a/o Gd H = 275 gauss

—— $LaAl_2$ matrix

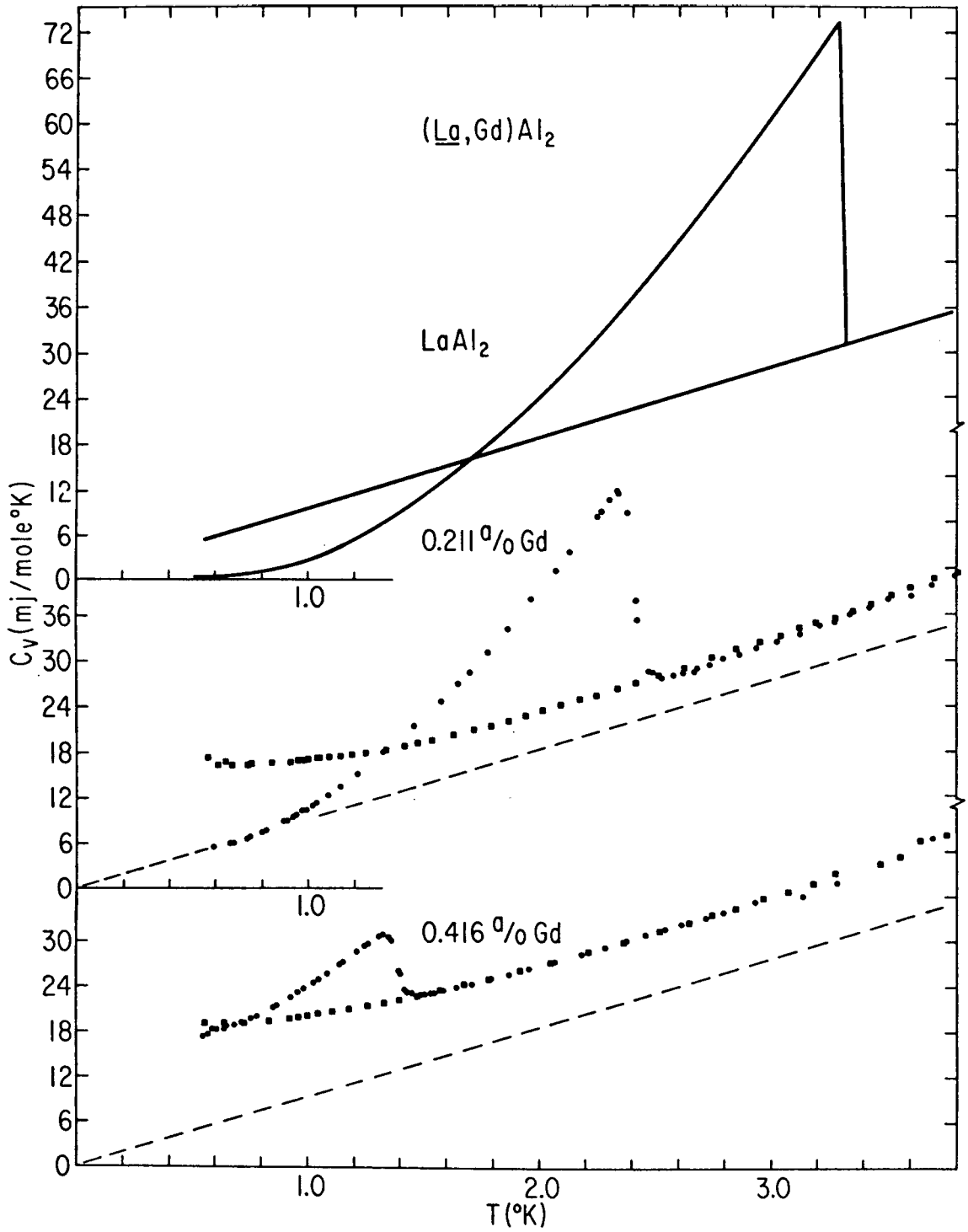
(La,Gd)Al2
LaAl2
0.211 a/o Gd
0.416 a/o Gd
Cv (mj/mole °K)
T (°K)
72
66
60
54
48
42
36
30
24
18
12
6
0
1.0
2.0
3.0

FIGURE 10

$C_s/\gamma T_c$ vs. T_c/T in the superconducting state (the βT^3 lattice contribution has been removed).

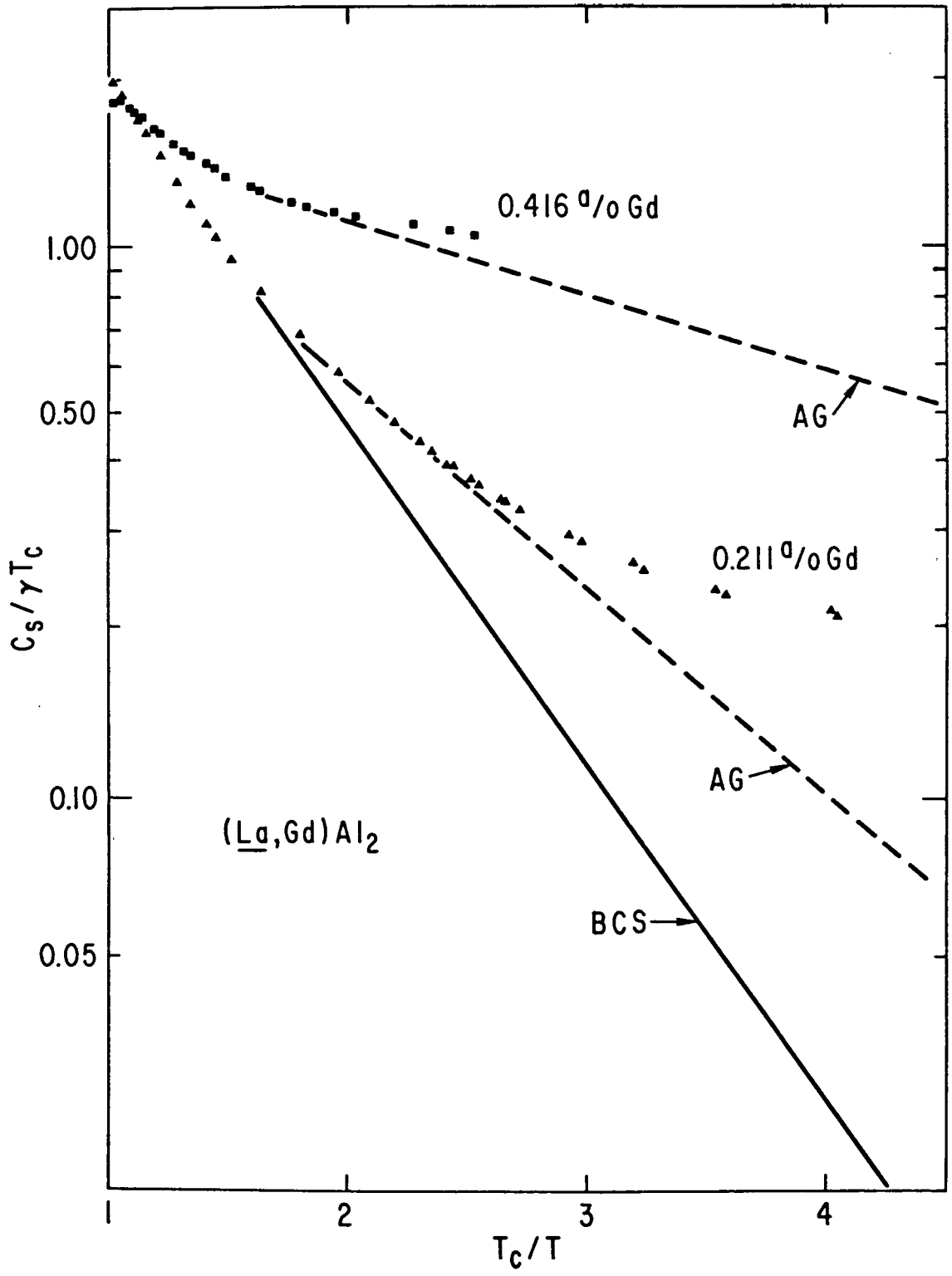
0.416 a/o Gd
AG
0.211 a/o Gd
AG
(La,Gd)Al2
BCS
1.00
0.50
0.10
0.05
Cs/γTc
1
2
3
4
Tc/T

FIGURE 11

C_v/T vs. T^2 in the normal state (the βT^3 lattice contribution has been removed).

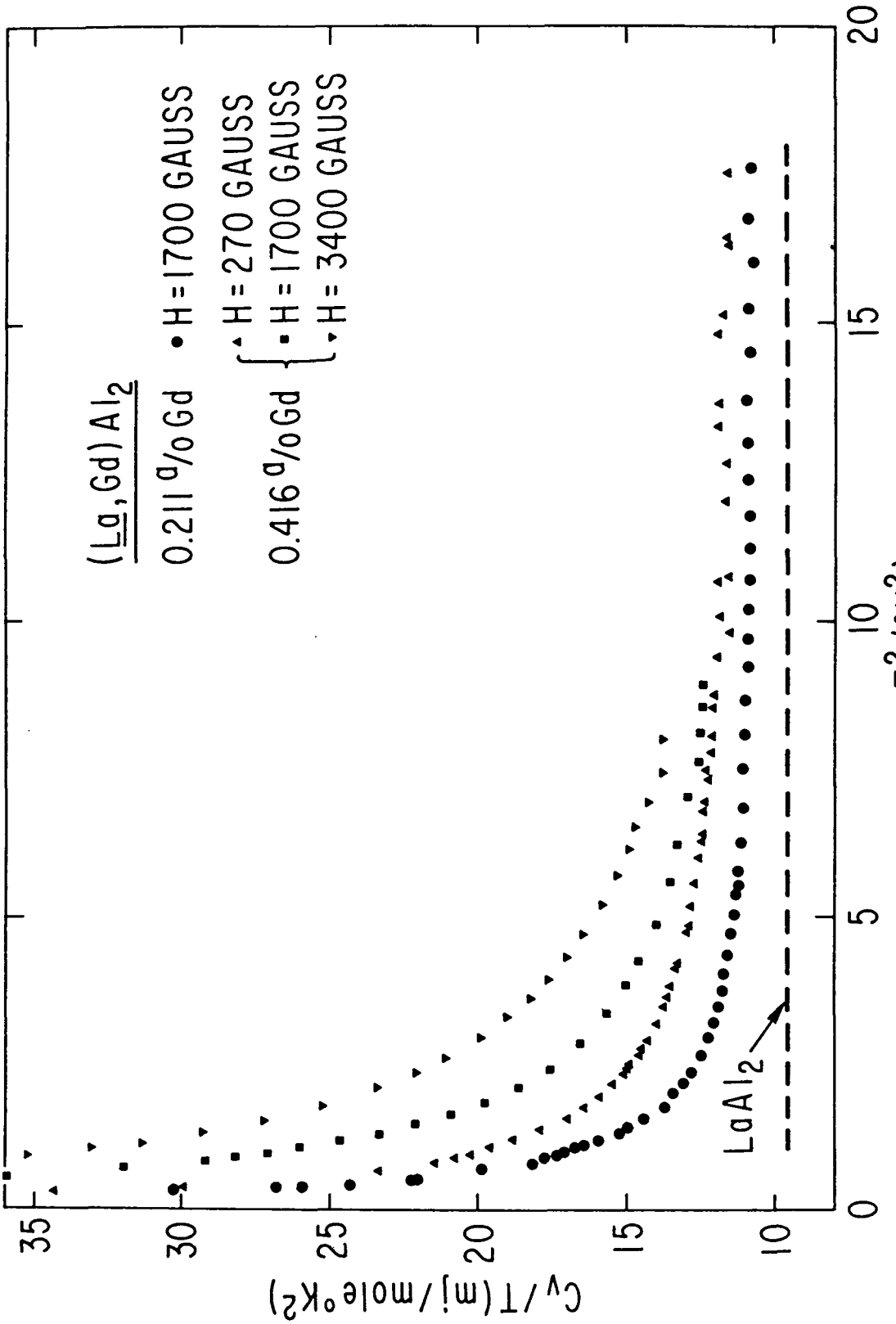
(La, Gd) Al2
0.211 % Gd • H = 1700 GAUSS
0.416 % Gd ▲ H = 270 GAUSS
■ H = 1700 GAUSS
▼ H = 3400 GAUSS
LaAl2
Cv/T (mj/mole °K2)
T2 (°K2)
10
15
20
25
30
35
0
5
10
15
20

FIGURE 12

Excess heat capacity δC due to exchange scattering in the normal state (the electronic and the lattice contributions have been removed). The behavior of ($\underline{La}$, Ce)Al_2 is shown for comparison (dashed line).

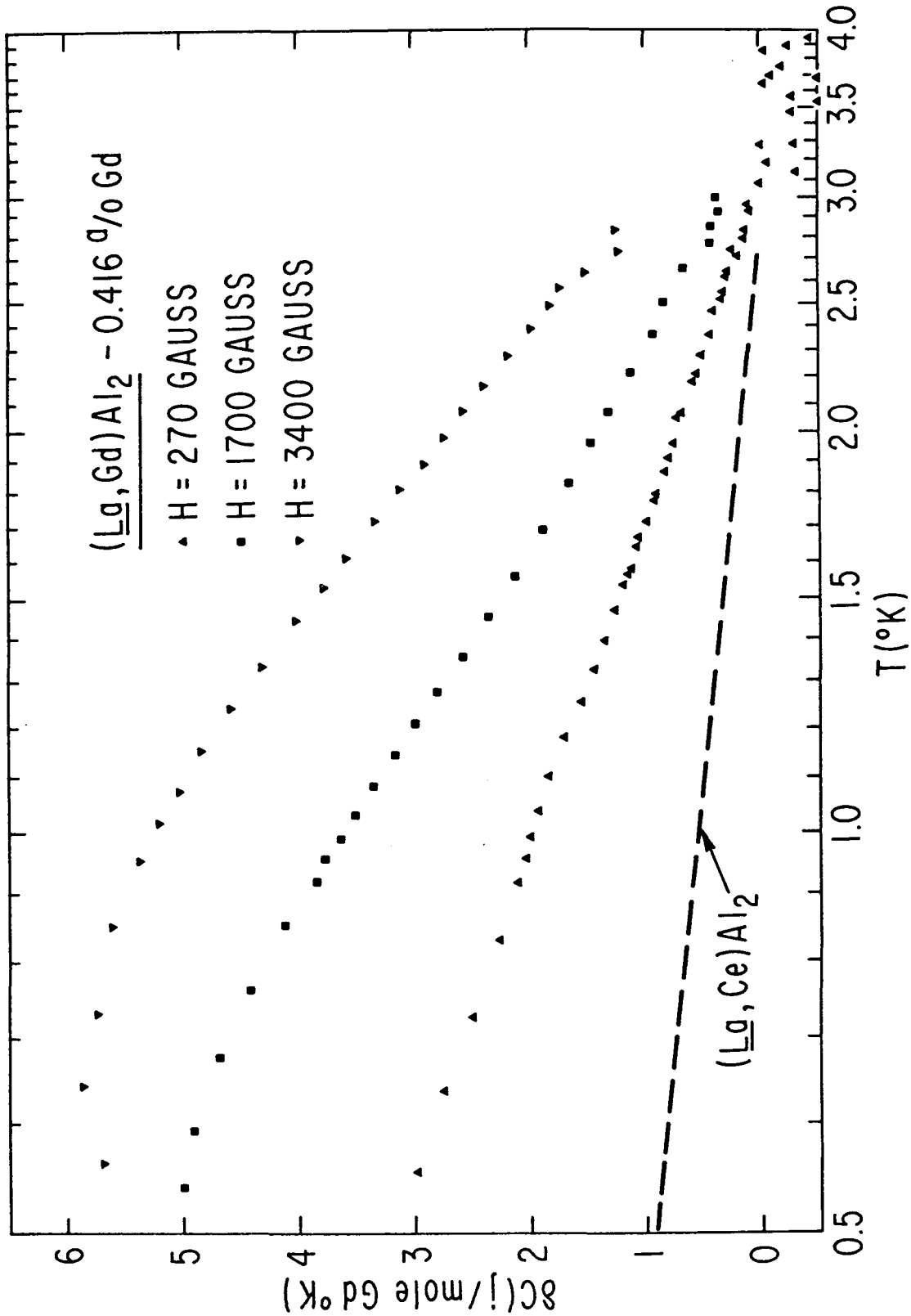
(La,Gd)Al2 - 0.416 a/o Gd
H = 270 GAUSS
H = 1700 GAUSS
H = 3400 GAUSS
(La,Ce)Al2
δC(j/mole Gd °K)
T(°K)
0
1
2
3
4
5
6
0.5
1.0
1.5
2.0
2.5
3.0
3.5
4.0

have ionic levels lying far below the Fermi level of the host, interacting with the conduction electrons via the exchange Hamiltonian (2) with a positive coupling constant J_{sl}. The data also suggest that the AG assumption of non-interacting, randomly distributed impurity spins is appropriate in describing the superconducting properties of these alloys.

The (La, Ce)Al_2* data seen in Fig. 13 show strong departures from the AG prediction. These departures of $\Delta C/\Delta C_o$ vs. T_c/T_{co} correlate with the striking re-entrant behavior observed for this system in the T_c vs. n curve (Fig. 1(a)) which results from the temperature dependence of the pair breaking parameter. The logarithmically temperature dependent magnetic contribution to the electrical resistivity for this system implies that the Ce impurity spins couple antiferromagnetically with the conduction electron spins giving rise to temperature dependent exchange scattering (Kondo effect). As we have discussed in the Introduction, the AG theory has been modified for the case of a negative coupling parameter J_{sl}; the pair breaking parameter α (independent of temperature in the AG picture) becomes strongly temperature dependent with a maximum at $T = T_o$. The magnitude of the depression of T_c and its detailed variation with impurity concentration depends on the ratio T_o/T_{co}

---

*Recent heat capacity measurements on the (La, Ce)Al_2 system made at the University of Cologne, Germany, are in general agreement with our measurements (F. Steglich, private communication).

(T_o is identified with T_K in the magnetic limit $T_o \ll T_{co}$). These calculations of T_c vs. n predicted for the limit $T_o \ll T_{co}$ a second transition back into the normal state which has been observed in the (La, Ce)Al_2 system. MHZ[55] calculated the specific heat within this theoretical framework. Their result for the initial slope

$$\left[\frac{d(\Delta C^*)}{dt_c^*}\right]_{t_{c=1}^*} = \left[\frac{d(\Delta C/\Delta C_o)}{d(T_c/T_{co})}\right]_{T_c/T_{co}=1}$$

(see Fig. 13) as a function of T_o/T_{co} has a maximum for $T_o \sim T_{co}$ which is almost a factor of two greater than the slope given by the AG theory. A self-consistent test is thereby obtained by fitting the T_c vs. n results and our results for $\Delta C(T_c)$ to the respective calculations, the characteristic temperature being the adjustable parameter. $T_o \sim 0.1°K$ obtained from the initial slope of the T_c vs. n plot,[30, 31] is in reasonable agreement with $T_o \sim 0.6°K$ deduced from our specific heat data.

The temperature dependent pair breaking picture has been pushed further to describe the observed T_c vs. n behavior of the ThU alloys as an example of the nonmagnetic limit of the theory ($T_o \gg T_{co}$) where the predicted T_c vs. n curve is nearly exponential in shape and single-valued. MHZ[28] and Ludwig and Zuckermann[29] (hereafter LZ) were able to fit the T_c data of Maple et al.[33] by

assuming a localized spin $S = 1/2$* at a U site and $T_o/T_{co} = 32$. However, the reasonable fit of our specific heat results to the BCS Law of Corresponding States (again, see Fig. 13) is incompatible with the MHZ calculation since the BCS limit is not reached in the pair breaking picture even when $T_o/T_{co} \rightarrow \infty$ ($[d(\Delta C^*)/dt_c^*]_{t_c^*} = 1$ approaches the AG value in this limit). The ThU results are better understood within the framework of pair weakening where the interactions responsible for the depression of the critical temperature T_c do not destroy the time reversal invariance responsible for the infinite lifetime of the Cooper pairs. The T_c vs. n behavior can be described very well by a modified exponential proposed by Kaiser[36] (Fig. 1(c)) to account for the effect of nonmagnetic resonant states on the superconducting properties of the host. This theory also predicts a BCS Law of Corresponding States as observed and previously reported for the related systems AlMn[56] and ThCe[57] which also exhibit modified exponential depressions of T_c with impurity concentration.

We turn now to discuss features of our specific heat data other than the jumps at T_c in zero field. The normal state heat capacity measurements on the (La, Ce)Al_2 and (La, Gd)Al_2 alloys

---

*The assumption of $S = 1/2$ for the low temperature nonmagnetic limit ($T_o >> T_c$) is not consistent with the high temperature ($T > T_o$) Curie-Weiss behavior observed in the susceptibility which gives an effective moment of 3.43 μ_B, close to the Hund's rule value of 3.58 μ_B for two 5f electrons.

have been made in magnetic fields to quench superconductivity. The zero temperature upper critical field $H_{c2}(0)$ reported for $LaAl_2$ from a.c. mutual inductance measurements is ~ 2.5 kgauss.[58,59] However, our measurements, performed in a field of 1.7 kgauss, failed to indicate bulk superconductivity down to 0.5°K (assuming a parabolic relationship for $H_{c2}(T)$ and the reported value $H_{c2}(0) \sim$ 2.5 kgauss a critical temperature of about 2.5°K is expected in a 1.7 kgauss field). We suggest that the reported values of the "upper critical field" may be associated with H_{c3}. Our observation is consistent with static magnetization vs. field measurements which give an $H_{c2}(0)$ value of about 1.5 kgauss.[66]

The fact that the critical fields of the alloys with Gd and Ce impurities are so drastically depressed relative to the critical field of the $LaAl_2$ matrix made plausible the use of relatively low magnetic fields to obtain the normal state data without introducing appreciable contributions from the field-induced Zeeman splitting of the impurity levels. Furthermore, the very low lattice contribution at liquid helium temperatures has also contributed favorably to the accurate determination of the magnitude and temperature dependence of the impurity contribution to the specific heat.

More evidence of Kondo anomalies in the (La, Ce)Al_2 system (besides those discussed in the preceding paragraphs and in the Introduction) in the (La, Ce)Al_2 system emerges from the normal

state specific heat results. That the magnetic field does not visibly affect the normal state heat capacity, and that the impurity contribution scales with concentration, supports the idea that the observed behavior is mainly a single impurity effect. The low temperature upturn of the heat capacity would appear to be the high temperature tail of an exchange scattering anomaly which should have a maximum near the characteristic temperature $T_o \cong 0.1°K$, similar to that observed in the CuCr alloys[7] ($T_o = 2.1°K$). Additional experiments at lower temperatures and stronger magnetic fields are desirable in order to study the nature of this anomaly.

An unexpected, surprisingly similar logarithmic upturn in the specific heat for $T < 3.5°K$ was found in the (La, Gd)Al_2 system (Figs. 11, 12). Measurements in various fields reveal the presence of a specific heat maximum which presumably occurs also in zero field at temperatures considerably lower than our temperature limit of 0.5°K. Kondo has calculated the entropy of an electron gas perturbed by the exchange scattering Hamiltonian (2) for $J_{sl} > 0$.[6] The calculated specific heat is a monotonically increasing function of temperature for $T < T_F$.* Therefore the low temperature anomaly in the (La, Gd)Al_2 system cannot be understood in this single-impurity exchange scattering picture. A search in the literature revealed that

---

*I am grateful to E. Galleani d'Agliano for drawing my attention to this point.

in the related $\underline{Y}Gd$[17] and $(\underline{La}, Gd)_3Al$[20] systems, maxima in the low temperature heat capacity have been observed and interpreted as evidence of impurity ordering (see page 7). The interpretation is more difficult in our experiments, since we have not determined the concentration dependence of the maximum. However, further information is gained since the heat capacity of these alloys is strongly dependent on the external field (Figs. 11, 12). Since the superconducting data suggested the presence of ionic, non-interacting magnetic moments, the magnetic field should have induced a Schottky anomaly in the impurity heat capacity peaked at a temperature $T_{max} \sim \mu H/k_B$, where $\mu \cong 7\mu_B$ is the Gd moment. In Fig. 14 we present the impurity heat capacity for a sample containing 0.416 a/o Gd in fields of 1.7 and 3.4 kgauss and, for comparison, the corresponding free-ion Schottky peaks. The clear disagreement suggests that correlations exist between Gd ions. The normal state results therefore seem to be Schottky-like anomalies due to an effective molecular field existing at the impurity sites. This effective field originates with the other impurities and proceeds via the long range RKKY oscillatory conduction electron spin polarization, resulting in a statistical distribution of fields apparently peaked at a value of the order several hundred gauss ($H_{eff} \sim k_B T_{max}/\mu$).

It is worthwhile to consider the apparent contradiction between the superconducting results which indicate the absence of

interactions and the normal state results which show a strong contribution due to impurity spin interactions. Figure 9 shows that the magnetic impurity contribution to the normal state heat capacity in the more concentrated sample (0.416 a/o Gd) has a tail which extends to temperatures higher than T_c and at T_c is approximately 25% of the total heat capacity. The fact that the jump is not depressed more than predicted by AG suggests that the specific heat jump is not sensitive to the type of ordering effects encountered here, at least when T_c is sufficiently greater than the temperature of the specific heat maximum ($< 0.5°K$ for the alloys measured here). These magnetic correlations are also visible in the superconducting state heat capacity (Fig. 11) and provide an experimental indication for the possible coexistence of magnetic ordering and bulk superconductivity at lower temperature. Further experiments in the dilute region will clarify the concentrating scaling, while measurements at lower temperatures and higher fields will provide information concerning the relationship between T_{max} and T_c at various Gd impurity concentrations.

Another peculiar phenomenon is the strong enhancement of the electronic specific heat coefficient γ which has been observed in both (La, Ce)Al_2 and (La, Gd)Al_2 alloys. Similar strong effects have also been reported in the related systems YGd and LaGd.[17] We disagree with the virtual bound state picture which was invoked in reference 17 since the hybridization is expected to be small in the ionic

regime encountered for Gd impurities, and only moderately large for Ce impurities in the strong magnetic limit $T_o/T_{co} << 1$. Also, rigid band effects are expected to be negligible in the dilute limit and are not in accord with the experimental result that the impurity contribution seems to be independent of concentration [$\Delta\gamma/n \neq f(n)$] . It can be argued that our temperature range does not extend high enough to differentiate between the linear behavior in T or a more complicated dependence associated with the low temperature anomaly; however in the earlier experiments on LaGd and YGd the temperature ranges extended up to 8°K and 35°K, respectively, throughout which a constant enhancement of γ was observed. We believe that the large enhancement of γ is more likely due to a strong polarization of the conduction electrons induced by the impurity spins via the exchange interaction (2) in the high temperature paramagnetic region.

The ThU results can best be understood within a frame of reference which includes in one class the three closely related systems ThCe, AlMn and ThU, listed in order of their increasing tendency towards magnetism. The susceptibility of ThCe[60] decreases below 300°K, indicating the absence of magnetism at low temperatures, while the susceptibility of AlMn[61] shows a temperature independent but large enhancement. The susceptibility of ThU[33] is strongly enhanced relative to that of pure Th and shows a weak, nearly Curie-Weiss dependence on temperature. The impurity

contribution to the residual resistivity of these three systems is described by the relation

$$\Delta\rho(T) = \Delta\rho(0)\,[1 - (T/T_o)^2]$$

which is characteristic of a scattering process between electrons and localized magnetic moments which fluctuate in time with a characteristic frequency[62]

$$\tau_{sf}^{-1} = \frac{k_B}{h} T_o$$

Intuitively we see that the lower T_o (the longer lived the local moments), the more magnetic the behavior attributed to the particular impurity. Again, as in the magnetic limit, the characteristic temperatures can be used to characterize the magnetic behavior; the normal state resistivities give $T_o > 1000$ K for ThCe,[63] ~ 530°K for AlMn[62, 34] and ~ 100°K* for ThU.[33] As seen the residual resistivity correlates with the susceptibility in indicating that ThU is closer to the magnetic regime. The detailed T_c vs. n curves for these systems show further similarity. In each case, with increasing impurity concentration, T_c falls off very fast as a modified exponential. Again the strongest effect is found for ThU.[35] However, for all

---

*The value of $T_o \sim 100$°K for the ThU system is also evident from the thermoelectric power which exhibits a maximum near 80°K.[33]

three systems, the specific heat jump at T_c follows the BCS Law of Corresponding States,* emphasizing their essentially nonmagnetic character at superconducting temperatures. An enhancement of the electronic specific heat coefficient, linear in concentration is expected in nonmagnetic systems. This impurity contribution is proportional to the density of states at the Fermi level of the virtual bound state localized at each impurity site. As first calculated by Klein and Heeger,[64]

$$\frac{d\gamma}{dn} = \frac{\pi^2}{3} k_B^2 N_l(E_F)$$

According to our results for the initial increase of γ, $N_f(E_F)$ is 57 states/eV atom U for the ThU system. In AlMn the corresponding value is $N_d(E_F)$ = 10 states/eV atom Mn.[65] The ratio $N_f(E_F)/N_d(E_F)$ = 5.7 is very similar to the inverse of the ratio between the corresponding characteristic temperatures. This relation between the specific heat and resistivity results can be understood in the framework of models[62] which attribute the weakly magnetic nature of these systems to localized spin fluctuations. In such models the half-width of the impurity level is narrowed by the presence of spin fluctuations to an effective value Δ_{eff}. T_o and $N_l(E_F)$ are expected to be of the order of Δ_{eff}/k_B and Δ_{eff}^{-1}, respectively, which accounts for the relation above.

---

*Critical field data for the ThU system, recently reported, show small departures from BCS behavior.[39]

FIGURE 13

Reduced specific heat jump $\Delta C/\Delta C_{co}$ versus reduced critical temperature T_c/T_{co}.

◆ - ThU alloys

■ - (La, Gd)Al_2 alloys

● - (La, Ce)Al_2 alloys

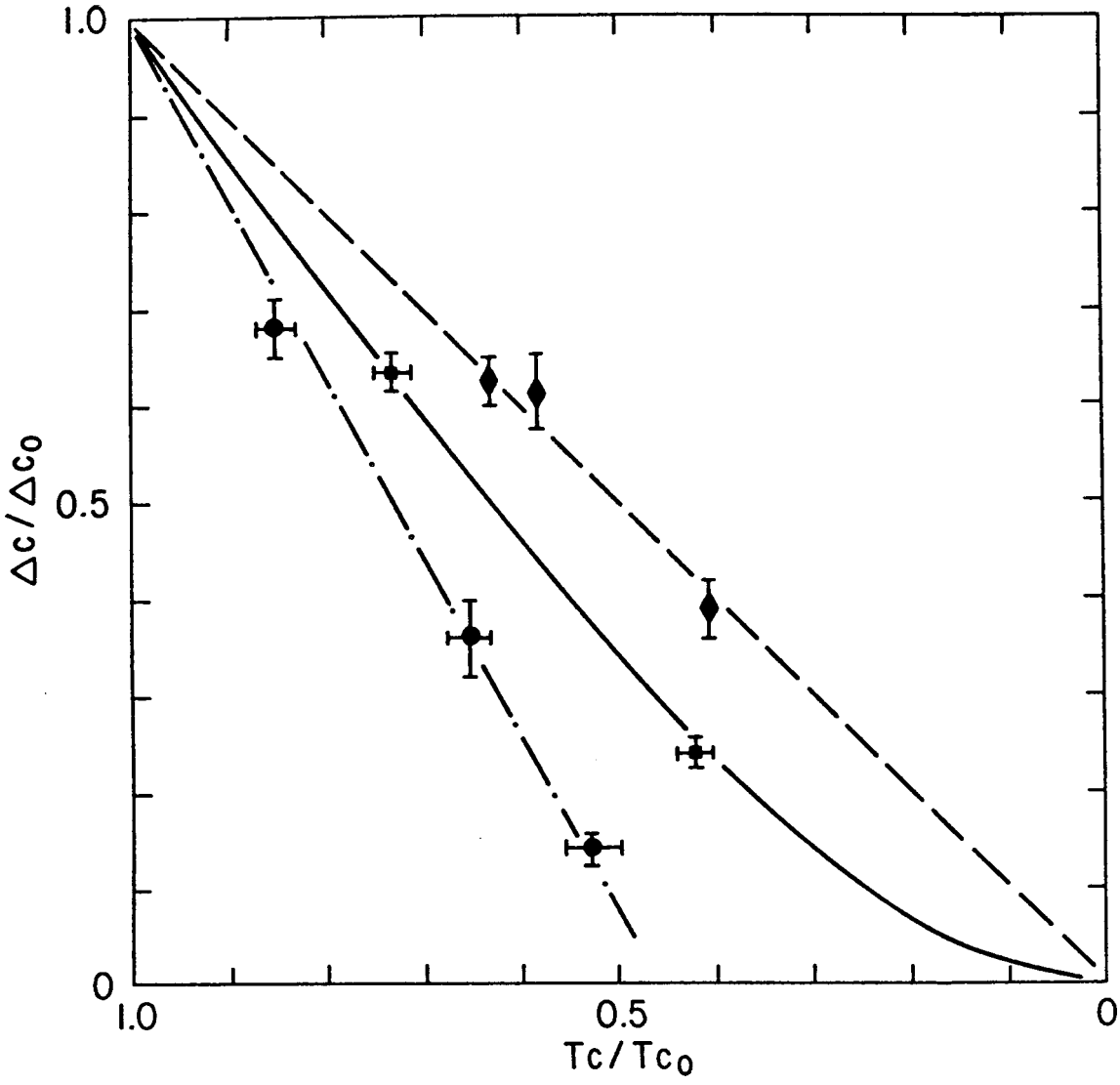
1.0
0.5
0
Δc / Δc0
1.0
0.5
0
Tc / Tc0

FIGURE 14

δC versus ln T. Magnetic field dependence of the magnetic impurity contribution in $(\underline{La}, Gd)Al_2$.

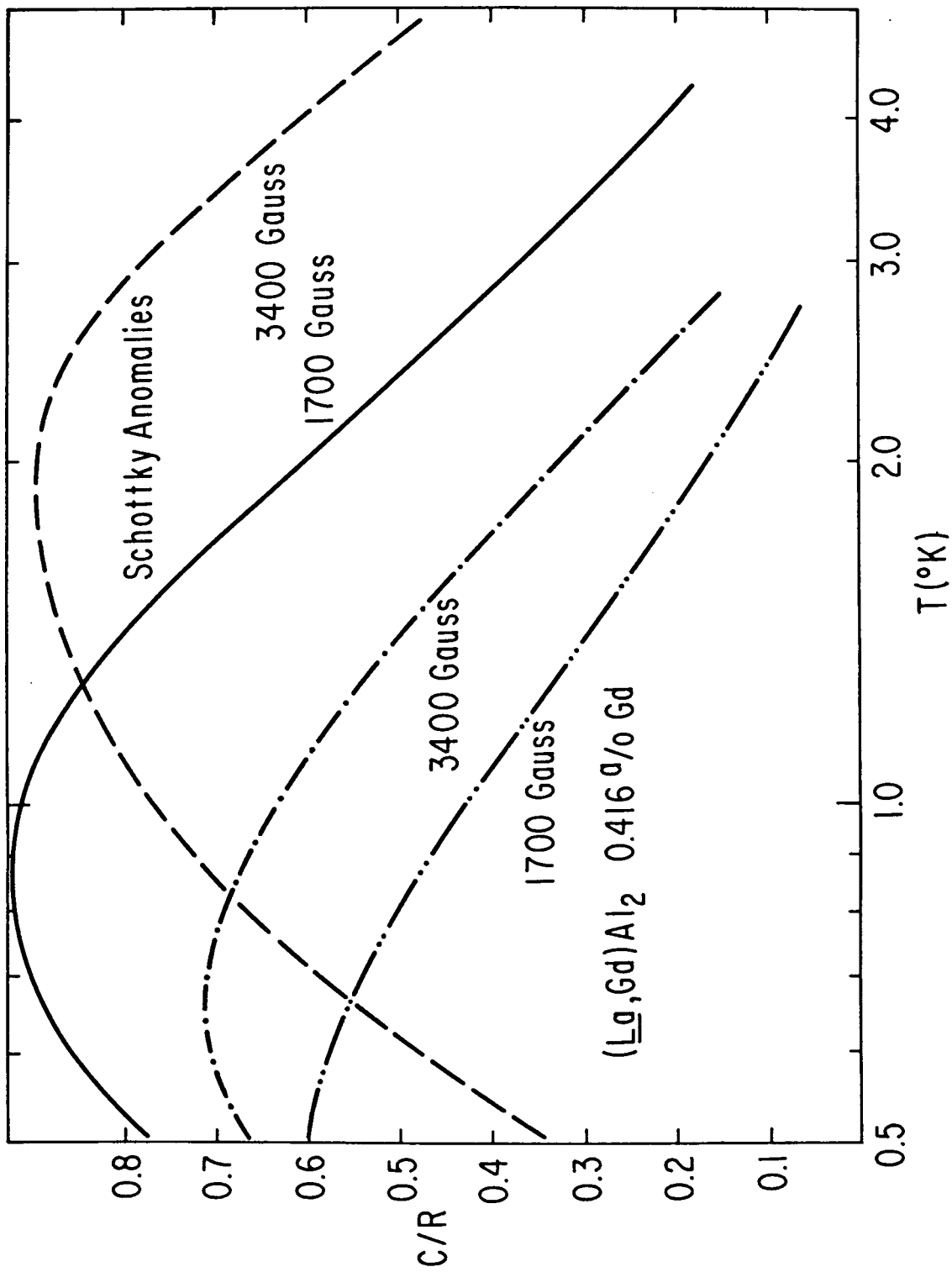
Schottky Anomalies
3400 Gauss
1700 Gauss
3400 Gauss
1700 Gauss
(La,Gd)Al2 0.416 a/o Gd
C/R
T(°K)
0.8
0.7
0.6
0.5
0.4
0.3
0.2
0.1
0.5
1.0
2.0
3.0
4.0

REFERENCES

1. J. Friedel, Can. J. Phys. 34, 1190 (1956); Nuovo Cimento (Suppl.) 7, 287 (1958); in "Metallic Solid Solutions" (J. Friedel and A. Guinier, eds.) Benjamin, New York (1963).

2. P. W. Anderson, Phys. Rev. 124, 41 (1961).

3. N. Rivier and M. J. Zuckermann, Phys. Rev. Letters 21, 904 (1968).

4. J. Kondo, Prog. Theor. Phys. 32, 37 (1964).

5. Y. Nagaoka, Phys. Rev. 138, A1112 (1965).

6. J. Kondo, in "Solid State Physics" (Seitz, Turnbull, and Ehrenreich, eds.) Academic Press, New York, Vol. 23, p. 183 (1969).

7. B. B. Triplett and N. E. Phillips, Phys. Rev. Letters 27, 1001 (1971).

8. J. R. Schrieffer and P. A. Wolff, Phys. Rev. 149, 491 (1966).

9. M. B. Maple, J. Wittig, and K. S. Kim, Phys. Rev. Letters 23, 1375 (1969); M. B. Maple and J. Wittig, Solid State Commun. 9, 1611 (1971).

10. G. Boato and C. Rizzuto, in "Proc. of the 11th Int. Conf. on Low Temp. Phys., St. Andrews, Scotland, 1968" (J. G. Allen, D. M. Findlayson, and D. M. McCall, eds.); J. G. Huber and M. B. Maple, to appear in the Proceedings of the 13th Int. Conf. on Low Temp. Phys., Boulder, Colorado (1972); J. G. Huber, Ph.D. Thesis (unpublished), University of California, San Diego (1971).

11. M. B. Maple and Z. Fisk, in Proc. of the 11th Int. Conf. Low Temp. Phys. (see Ref. 10).

12. See, for example, "Quantum Theory of Solids," C. Kittel, John Wiley & Sons, Inc., 1963.

13. M. A. Ruderman and C. Kittel, Phys. Rev. 96, 99 (1954); K. Yosida, Phys. Rev. 106, 893 (1957); T. Kasuya, Prog. Theor. Phys. (Kyoto) 16, 45 (1956).

14. W. Marshall, Phys. Rev. 118, 1519 (1960).

15. M. W. Klein, J. Appl. Phys. 35, 944 (1964).

16. S. H. Liu, Phys. Rev. 157, 411 (1967).

17. J. Bonnerot, B. Caroli, and B. Coqblin, Ann. Acad. Sci. Fennicae AVI, 120 (1966).

18. F. J. Du Chatenier and J. De Nobel, Physica 32, 1097 (1966).

19. J. Souletie and R. Tournier, J. Low Temp. Phys. 1, 95 (1969).

20. T. Mamiya, T. Aoi, K. Iwahashi, and Y. Masuda, J. Phys. Soc. Japan 31, 485 (1971).

21. P. Costa Ribeiro, M. Saint Paul, D. Thoulouze, and R. Tournier, to appear in the Proceedings of the 13th Int. Conf. on Low Temp. Phys., Boulder, Colorado (1972).

22. B. T. Matthias, H. Suhl, and E. Corenzwit, Phys. Rev. Letters 1, 92 (1958).

23. R. A. Hein, R. L. Falge, B. T. Matthias, and E. Corenzwit, Phys. Rev. Letters 2, 500 (1959).

24. M. B. Maple, Ph.D. Thesis (unpublished), University of California, San Diego (1969).

25. A. A. Abrikosov and L. P. Gor'kov, Zh. Eksp. i Teor. Fiz. 39, 1781 (1960); Soviet Phys. JETP 12, 1243 (1961).

26. M. B. Maple, Phys. Letters 26A, 513 (1968).

27. R. P. Guertin, Ph.D. Thesis (unpublished), University of Rochester (1968).

28. E. Müller-Hartmann and J. Zittartz, Phys. Rev. Letters 26, 428 (1971).

29. A. Ludwig and M. J Zuckermann, J. Phys. F: Metal Phys. 1, 516 (1971).

30. G. Riblet and K. Winzer, Solid State Commun. 9, 1663 (1971).

31. M. B. Maple, W. A. Fertig, A. C. Mota, L. E. DeLong, D. Wohlleben, and R. Fitzgerald, Solid State Commun. 11, 829 (1972).

32. M. B. Maple, AIP Conference Proceedings (No. 4) on "Superconductivity in d- and f-Band Metals" (edited by D. H. Douglass), pp. 175-203 (1972).

33. M. B. Maple, J. G. Huber, B. R. Coles, and A. C. Lawson, J. Low Temp. Phys. 3, 137 (1970).

34. E. Babic, P. J. Ford, C. Rizzuto, and E. Salamoni (to be published).

35. J. G. Huber and M. B. Maple, Solid State Commun. 8, 1987 (1970).

36. A. B. Kaiser, J. Phys. C3, 409 (1970).

37. J. Bardeen, L. N. Cooper, and J. R. Schrieffer, Phys. Rev. 108, 1175 (1957).

38. As calculated by S. Skalski, O. Betbeder-Matibet, and P. R. Weiss, Phys. Rev. 136, A1500 (1964).

39. H. L. Watson, D. T. Peterson, and D. K. Finnemore, to appear in the Proceedings of the 13th Int. Conf. on Low Temp. Phys., Boulder, Colorado (1972).

40. C. A. Luengo, J. M. Cotignola, J. G. Sereni, A. R. Sweedler M. B. Maple, and J. G. Huber, Solid State Commun. 10, 459 (1972).

41. This set of samples was prepared by John Huber in La Jolla.

42. C. A. Luengo, J. M. Cotignola, J. Sereni, A. R. Sweedler, and M. B. Maple, to appear in the Proceedings of the 13th Int. Conf. on Low Temp. Phys., Boulder, Colorado (1972).

43. This set of samples was prepared by A. R. Sweedler in the Facultad de Ciencias, Universidad de Chile.

44. J. E. Gordon, H. Montgomery, R. J. Noer, G. R. Pickett and R. Tobón, Phys. Rev. 152, 432 (1966).

45. W. R. Decker and D. K. Finnemore, Phys. Rev. 172, 430 (1968).

46. M. Saint Paul, J. Souletie, D. Thoulouze, and B. Tissier, J. Low Temp. Phys. 7, 129 (1972).

47. The purity analysis of the dealer indicated a main impurity content of 100 ppm Ce.

48. The samples were prepared by M. B. Maple. This set of experiments was made in calorimeter III built in La Jolla.

49. M. B. Maple, W. A. Fertig, A. C. Mota, L. E. DeLong, D. Wohlleben, and R. Fitgerald, Solid State Commun. 11, 829 (1972).

50. C. A. Luengo, M. B. Maple, and W. A. Fertig, Solid State Commun. (forthcoming).

51. H. V. Culbert and A. S. Edelstein, Solid State Commun. 8, 445 (1970).

52. These samples were prepared by M. B. Maple. This set of experiments was made in calorimeter III built in La Jolla.

53. M. B. Maple, private communication.

54. C. A. Luengo and M. B. Maple (to be published).

55. E. Müller-Hartmann and J. Zittartz, Solid State Commun. 11, 401 (1972).

56. D. L. Martin, Proc. Roy. Soc. (London) 78, 1489 (1961); F. W. Smith, J. Low Temp. Phys. 6, 435 (1972).

57. C. W. Dempesy (unpublished). See Ref. 32.

58. G. Riblet and K. Winzer, Solid State Commun. 11, 175 (1972).

59. D. Davidov, A. Chelkowski, C. Rettori, R. Orbach, and M. B. Maple, Phys. Rev. (forthcoming).

60. L. F. Bates and M. M. Newmann, Proc. Phys. Soc. 72, 345 (1968).

61. F. T. Hedgcock and P. L. Li, Phys. Rev. B2, 1342 (1970).

62. A. D. Caplin and C. Rizzuto, Phys. Rev. Letters 21, 746 (1968).

63. J. R. Cooper and C. Rizzuto (to be published).

64. A. P. Klein and A. J. Heeger, Phys. Rev. 144, 458 (1966).

65. R. Aoki and T. Ohtsuka, J. Phys. Soc. Japan 23, 955 (1967).

66. M. B. Maple, private communication (unpublished).

II. THE CALORIMETERS

A. INTRODUCTION

The heat capacity experiments were made in three calorimeters successively built during this research. The basic design is an unusual variation of the heat pulse technique widely used in adiabatic calorimetry at low temperatures. The sample is usually isolated from the heat sink with nylon threads in a vacuum container immersed in the helium bath. This isolation system is efficient in preventing conduction heat leaks to the surroundings. To cool the sample, a mechanical heat switch is widely used in the He^3 and He^4 temperature ranges. Since this suspension system is very sensitive to vibrational heating, mechanical actions on the sample are undesirable. Consequently, most switches are jaw shaped acting on a metallic contact thermally linked to the sample (Fig. 1, a).[1,2] Alternatively, the sample can be rigidly suspended by some insulating material. This solution is relatively more insensitive to vibrations and, because of the rigid suspension, the force needed for efficient thermal contact can be directly applied to the sample with consequent advantages in design and handling (Fig. 1, b). In addition, the temperature of the sample can be easily controlled because of the relatively high thermal conductance of the suspension system. Also, the problems arising from misalignment of the contacts in the switch jaws

can be eliminated, resulting in a minimization of the heat input when opening the switch.

In the following we describe three semi-adiabatic calorimeters which are operated in the He^3 and He^4 temperature ranges. We also discuss in some detail the limitations of the semi-adiabatic method.

B. TECHNICAL DESCRIPTION

Calorimeter I

The main features of this calorimeter, built in Bariloche, include a mechanical heat switch operated by a bellows and a semi-adiabatic method for thermal isolation of the sample. A diagram of this calorimeter is shown in Fig. 2. Four nylon screws isolate the sample and addenda (e) from the sample holder (c). Conduction heat leaks through the screws are minimized by controlling the temperature of the sample holder so that it is close to that of the sample. The sample is cooled by pumping both the He^4 (a) and He^3 (b) refrigerators. Thermal contact to the He^3 reservoir is obtained with a heat switch consisting of a 0.002" copper foil (g) glued to the sample with GE 7031 varnish, and pressed against the He^3 thermal sink (h). The force is applied with the bellows (j) which is actuated with liquid He^4 at high pressures.[3] Partial thermal isolation between the bellows at superfluid He^4 temperatures and the He^3 thermal sink is obtained with a piece of nylon (i) of high thermal impedance.

In spite of successful measurements on the AgZn system,[4] some design changes were deemed necessary for the following reasons:

a) We were not able to cool the sample below 0.7°K due to the combined effect of the thermal resistance of the contact and the heat conducted through it and the nylon piece (i).

b) Having to glue the addenda to the sample for each experiment introduces a certain degree of uncertainty due either to possible alterations of the resistor calibration or small changes in the heat capacity of the addenda.

c) Good alignment of the copper foil in the thermal switch was difficult to obtain; some experiments failed simply because the foil touched either (h) or (i) in Fig. 2. Also, suspension of the samples with screws (f) was impractical for the new, irregularly shaped samples.

Calorimeter II

A diagram of Calorimeter II is shown in Fig. 3. The sample (0) is contained in a gold plated copper cylinder about 7 cm^3 in volume. The lower end of the cylinder is a cap that, when screwed into place, insures thermal contact between sample and addenda (P). A 0.002" manganin heater (N) is wound and glued with GE 7031 to the cylinder. The germanium thermometer (K) is tightly pressed into a

gold plated copper capsule. Electrical leads are soft soldered to the heater wires. Heater voltage leads are 0.002" manganin wire and current leads are of superconducting lead coated manganin wire. A rigid 0.005" walled nylon cylinder is used to suspend the sample in this semi-adiabatic method. Heat leaks are minimized by controlling the temperature of the heat sink (dashed area in Fig. 3). A mechanical heat switch is used to cool the sample from 77°K to 0.35°K. A bellows (F), activated with He^4 pressure up to 3 atmospheres, pushes down on a nylon rod (G), the lower end of which is the contact (J) thermally linked to the He^3 heat sink. When the bellows is evacuated, the copper-beryllium spring (L) opens the switch. During calibration runs the switch is also used to provide thermal contact between the germanium thermometer and the magnetic thermometer. A He^4 heat exchanger is used to cool the calorimeter from 77°K to 4°K.[5] He^4 gas precooled in the main bath is circulated through copper tubing softsoldered to the heat sink (B). When the system is at 4°K, the tubing is evacuated and further cooling is obtained by circulating the He^3 through the refrigerator, precooled in the He^4 evaporator. Finally, 0.35°K is reached by pumping the condensed He^3. The 77°K to 4°K cooling time is less than three hours, while from 4°K the lowest temperature is reached in less than 30 minutes.

This calorimeter continues to work quite satisfactorily in Bariloche and its basic design was modified only slightly during construction of a third calorimeter in La Jolla.

Calorimeter III

In this case we wanted to make a single compact plug-in unit to be used in a conventional multipurpose dewar with pumping systems for He^3 and He^4. The suspension of the sample is essentially the same as previously described, except for the addenda whose heat capacity was minimized.

A simple He^3 heat exchanger combined with an air pressure operated heat switch allows a sample to be cooled from 77°K to 0.5°K in 1.5 hours. A controlled flux of He^3 gas is continuously circulated through the pumping system, the condenser (h) (see Fig. 4), the 1/64 I.D. copper-nickel capillary tube (j) and the He^3 refrigerator (l). When the sample (r) has been cooled down to 4°K the bath is pumped until the He^3 is condensed. The lowest temperature is reached by closing a valve at the gas inlet. The heat exchanger can also be operated with He^4 down to 1.5°K.

The upper end of the gold-plated copper contact (o) is immersed in the He^3 reservoir (l) which is an extendable bellows. When air is applied to the upper bellows (b), small longitudinal displacements are transmitted by the 5/32" stainless steel tube to the thermal contact (o) and the sample is then connected to the thermal sink. A 0.5 cm^3 copper bulb, hard soldered to the He^3 copper plate, is used either with He^3 or He^4 to calibrate the carbon and germanium resistors.

C. SEMI-ADIABATIC CALORIMETRY

The successful operation of a semi-adiabatic calorimeter requires that the temperature drift of the sample after the heating pulse $\dot{T}_s$ be small. We discuss this condition later, but if it holds, it is possible to extrapolate the temperature drift to the midpoint of the heating interval and then make an accurate determination of the temperature jump (see Fig. 5). $\dot{T}_s$ may be calculated to a good approximation by the expression

$$\dot{T}_s = \frac{\dot{Q}}{C} \tag{1}$$

where $\dot{Q}$ is the heat flux through the nylon cylinder (Fig. 1, b) and C is the effective heat capacity of the sample and its support. If C_s and C_{ny} are the heat capacities of the sample and nylon support, respectively, then $C = C_s\, C_{ny}/(C_s + C_{ny})$ as deduced from direct analogy to an electrical circuit. $\dot{Q}$ is calculated from

$$\dot{Q} = \frac{1}{R}\, \Delta T \tag{2}$$

where ΔT is the temperature jump of the sample (initially in thermal equilibrium with the heat sink) and R is the thermal resistance of the nylon cylinder. The resistance of the metallic sample, being much smaller, is neglected. Combining (1) and (2), the following expression is obtained

$$\dot{T}_s = \frac{\Delta T}{RC} = \frac{\Delta T}{\tau} \qquad (3)$$

τ, equal to RC, is a thermal time constant which is strongly dependent on temperature and can be evaluated from the thermal conductivity and specific heat data for nylon,[6,7] and from the heat capacity of the sample. For one mole of copper, our calculated time constant changes from 50 sec at 0.5 °K to 2000 sec at 5 °K. In units of the temperature jump, the expected temperature drifts are 8%/min and 3%/min, respectively. The measured drifts agree within 10% at high temperatures, while they are three times lower than expected at 1 °K, suggesting that the thermal contact resistance of nylon-copper is very large, and of the order of 30 °K/μ watt. The fact that the drifts are so small insures the good quality of the specific heat measurements (Fig. 5).

D. MECHANICAL HEAT SWITCHES

The heat switches are a critical point in low temperature calorimetry. The sample needs to be cooled down in a reasonable amount of time to the lowest temperature and then must be isolated from the cooling bath in order to make the measurements. In the early heat capacity experiments, helium exchange gas was used to cool the sample followed by extensive pumping to isolate it from the bath. Somewhat later it was realized that this technique introduced serious errors in the determination of small heat capacities due to the

heat of adsorption of the exchange gas. Nowadays mechanical heat switches are mostly used at He^3 and He^4 temperatures. The more efficient the switch is, the faster the cooling. A few parameters can be used to characterize the switches for comparison purposes. The heat conductance of the contacts is important and also the heating generated in opening the switch at the lowest temperature. Typically, loads as big as 1.5 kgm were applied directly onto the sample to make the thermal contact as described in section II. B. However, up to 3.5 kgm loads were supported without damage to the nylon cylinder.

Different heat inputs were observed when opening the switches at the lowest temperature. A maximum of 90 ergs was delivered to the sample when the second switch (Fig. 3) was closed at nitrogen temperatures, but if first operated at 4°K,[8] this quantity was reduced to about 30 ergs. The third switch (Fig. 4) introduced heat inputs as low as 7 ergs. These data were taken without attempting to optimize the performance of the heat switches.

The choice of the contacts plays an important role in the performance of the switch[8] and some data is available on the thermal conductance of different contacts. The switch used in calorimeter II has brass-gold plated copper contacts while that used in calorimeter III has gold-gold contacts. The thermal conductance $\varkappa$ of the switches was calculated from the expression*

*The thermal conductance of the support, being much smaller (Fig. 6), has been neglected.

$$\kappa = \frac{\dot{Q}}{\Delta T} \tag{4}$$

A heat flux $\dot{Q}$ was delivered through the contact by the heater located on the sample. When the steady state was reached, the temperature difference between sample and bath ΔT, was measured with a Cryocal germanium resistor on the sample and a precalibrated Speer carbon resistor located in the heat sink (Figs. 3, 4). The temperature was controlled by the regulator on the radiation shield. When the thermal conductance of a contact was too small to be measured in the above way, a dynamical method was employed. A heat pulse was delivered to the sample and the subsequent drift $\dot{T}_s$ was recorded. The thermal conductance was again determined from relation (4) but ΔT was assumed to be the temperature jump in the sample (since the temperature of the heat sink should not change under small heat inputs) and $\dot{Q}$, the heat flux, was calculated using

$$\dot{Q} = C \dot{T}_s \tag{5}$$

where C is the known heat capacity of the sample and $\dot{T}_s$ is the initial drift after the heat pulse. As the thermal conductance has a strong dependence on the force applied to the contacts, the results shown in Fig. 6 were normalized to a 1 kgm load. The force was estimated from the pressure applied to the driving bellows. The results for our Au-Au contacts are seen to be fairly similar to those previously reported by Hill and Pickett[8] for their switch, also with

Au-Au contacts. Their estimated force however, is several kgm, and the coincidence seems rather fortuitous since the value at 4°K increases more than 10% when the force is only 2 kgm. The reader may note that the thermal conductance for the brass-gold contact is between 5 and 10 times smaller for similar applied forces.

E. MEASURING SPECIFIC HEATS

The heat capacity experiments were performed with the heat pulse technique. The temperature jump in the thermally isolated sample was determined after the heat pulse was introduced. If the mass of the sample is known, its heat capacity is calculated from the expression

$$C_v = m^{-1} (\Delta Q/\Delta T) \qquad (6)$$

The joule heat input ΔQ is in turn given by

$$\Delta Q = (I^2 R)\ \Delta t$$

where R is the resistance of the manganin heater, measured to better than one part in one thousand and chosen to be about $100\,\Omega$. I is the heating current determined by measuring the potential drop across a $1000\,\Omega$ standard resistor with a digital voltmeter and Δt is the heating interval measured with a digital clock simultaneously triggered with the heating current by a double microswitch, for which simultaneity had been tested to be better than 1 millisec. The temperature

jump varied from 40 to 100 m°K depending on the temperature. The minimum heating rates changed from 4 erg/sec to 300 erg/sec in the range of measurement. These rates were used when measuring the heat capacity of the addenda, as small as 80 μj/°K at 0.5 °K.

The most delicate problem in this type of measurement is the thermometry. To make the temperature measurements, a 33 cps Wheatstone bridge was balanced at the desired initial value of the thermometer resistance; after heating the bridge was balanced again (Fig. 5). The temperature drift of the sample introduces small corrections δR to the equilibrium value R, which are calculated from the relation

$$\delta R = \alpha(R)\, \delta V$$

where δV is the change in the output voltage which corresponds to small changes in the equilibrium resistance. The parameter $\alpha(R)$ is determined for each value of the equilibrium resistance for known unbalances. The temperature jump is related to the total change in resistance ΔR in each specific heat point through the expression (see Fig. 5).

$$\Delta T = T(R_f) - T(R_i) = \frac{\partial T}{\partial R}\, \Delta R \qquad (7)$$

The function $T(R)$ has to be determined empirically by calibrating the resistance against the standard thermometers available in different ranges of temperature. We describe below the techniques

and procedures used during the calibration experiments.

Calorimeter I

This calorimeter was used in the liquid He^4 range from 1.4°K to 4.2°K.[4] For a thermometer an Allen Bradley 15Ω, 1/10 watt carbon resistor was calibrated against the vapor pressure of He^4 with temperatures determined from the He^4 1958 Temperature Scale.[9] The resistor was calibrated after each specific heat experiment. He^4 exchange gas was admitted into the vacuum jacket; then the main bath was progressively pumped down to 1.4°K. About 25 calibration points were taken at intermediate temperatures, the pressure of the bath being stabilized by controlling the pumping speed with a modified Walker regulator.[10] The vapor pressure, measured with mercury and oil manometers was that in the He^4 evaporator (Fig. 1) located close to the sample, which, used in this way acts as a bulb to avoid hydrostatic corrections. A least squares analysis of the data was made with the interpolation formula

$$\frac{1}{T} = \sum_{-3}^{+3} a_i (\ln R)^i \qquad (8)$$

The maximum relative deviation from the calculated values was 2×10^{-3} (Fig. 7(a)). The limits in the sum above were changed to obtain different expressions, the best fitting being obtained with this formula.

A 0.8 mole copper sample was measured to check the calorimeter. The copper was supplied by the American Smelting and Refining Co. (ASARCO) and measured "as received." About 80 experimental points were fitted to the usual formula

$$C_v = \gamma T + \beta T^3 \qquad (9)$$

The values of γ and β as deduced from the least squares analysis are shown in Table I. The measured Debye temperature agrees well with the value accepted as standard[11] while the coefficient of the linear term is about 5% larger.

Calorimeter II

The Allen Bradley 15Ω carbon resistor was found to be a satisfactory choice when working in the He^4 range; however its resistance is too high at low temperatures (approaching 400 kΩ at 0.3°K, see Fig. 8), so a less sensitive resistor was chosen to work between 0.35°K and 4.0°K. A Speer 470Ω, 1/2 watt, Grade 1002 carbon resistor was calibrated in the He^4 range as previously described. Below 1.4°K, a Cerium Magnesium Nitrate (CMN) thermometer was used as the standard. The paramagnetic susceptibility of the CMN, which is known to obey a Curie law down to 0.006°K,[12] was measured as the change in the mutual inductance of a compensated set of coils immersed in the He^4 bath.[13] This change in mutual inductance ΔM was related to the temperature T, through the expression

$$\Delta M = \frac{19.07 \pm 0.007}{T} \mu Hy°K \qquad (10)$$

as deduced from the least squares analysis of the data between 1.4°K and 2.5°K. ΔM was measured with a 17 cps inductance bridge[14] with a sensitivity of 4×10^{-4} at 1.0°K, and T determined from a pre-calibrated germanium resistor. Expression (10) was then extrapolated below 1.4°K and the resistor was in turn calibrated against the CMN.

A very simple interpolation function can be used with the Speer 470Ω carbon resistor[15]:

$$T = \frac{A}{(\ln R - B)^C} \qquad (11)$$

The constants in the expression above can be calculated from the experimental data with a desk calculator. The calibration points were fitted with a maximum relative deviation of 2×10^{-3} (Fig. 7(b)). The same copper sample was measured to test this calorimeter. In order to remove possible anomalies due to trapped gases,[16] the sample was annealed at 840°C for 100 hrs in a vacuum of 10^{-5} torr. About 50 specific heat points were taken between 0.4°K and 4.0°K and fitted to formula (9). The resulting values for the coefficients are presented in Table I.

After these preliminary experiments were made, new germanium resistors of higher reproducibility and sensitivity[17] became

available in our laboratory. A Cryocal 250Ω [18] germanium resistor was used in most of the experiments presented here. The same procedure was used to calibrate this resistor in the He^4 and He^3 ranges. A precalibrated Cryocal 1000Ω resistor was used as a standard above 4.0°K. The two resistors were mounted on the addenda (Fig. 3) and the manganin wires were thermally linked to the same point. It was found that differential heat conduction through the resistor wires can affect the thermal equilibrium of the sensing element of the resistor due to the finite thermal conductance to the surroundings. [19] Two different expressions were used to fit the data

$$\frac{1}{T} = \sum_{0}^{n} a_i (\ln R)^i \quad , \tag{12}$$

and

$$\ln T = \sum_{0}^{n} a_i (\ln R)^i \tag{13}$$

A least squares analysis of the data made for n increasing from 5 to 12 showed that the same rms deviation can be obtained with one coefficient less when formula (13) is adopted. About 63 calibration points were fitted to this expression with a maximum relative deviation of 2×10^{-3} (Fig. 7(c)). Only seven coefficients were needed in spite of the wide range in resistance values (Fig. 8).

The comparison of the fitting of the calibration data for these first three resistors (Fig. 7(a), (b), (c)) shows that maximum deviations

occur in the vicinity of the lambda point. After attempting several experimental procedures in order to optimize the thermal equilibrium between the sample and the He^4 evaporator where the vapor pressure readings were made, it was concluded that a different experimental arrangement was necessary to improve the equilibrium above 2.17°K. Also small systematic deviations can be observed when the magnetic and the vapor pressure scales are superimposed; they are due to the relatively larger uncertainty in measuring the magnetic temperatures. These deviations were finally removed by extending the calibration of the CMN to lower temperatures where the magnetic thermometer is more sensitive.

Calorimeter III

Most of the thermometry in this calorimeter was based on the vapor pressures of liquid He^4 or He^3 within a 0.5 cm^3 bulb hard soldered to a copper plate inside the vacuum jacket (Fig. 4). During calibration runs the thermometers, Speer 470Ω carbon and Cryocal 250Ω germanium resistors, were mounted on the copper plate. Charges of He^4 or He^3, depending on the temperature range, were condensed into the bulb. Between 2.0°K and 4.2°K, it was He^4; from 2.0°K, down to 0.7°K, it was He^3. Vapor pressure readings were made with mercury and oil manometers and the corresponding temperatures were determined from the He^4 1958 and He^3 1962 Temperature Scales.[9,20] Below 1.4°K, the plate was, of course, thermally

isolated from the He^4 bath by a vacuum, but above 1.4°K, exchange gas was admitted into the jacket and the bath was allowed to warm very slowly. Temperature equilibrium was established to better than 1 m°K/min by a cartesian manostat[21] when actually making vapor pressure readings. Between 0.7°K and 0.5°K the temperatures were determined by extrapolating the calibration function of the Speer 470Ω resistor[22] previously determined in the He^3 range. For the new Cryocal 250Ω resistor about 55 calibration points were fitted to expression (13) between 0.5°K and 4.2°K. Again the number of coefficients was seven but the fitting improved by a factor of two compared with the previous data (Fig. 7(d)). It is important to notice that the deviations characteristic of the lambda point have almost disappeared.

F. CONCLUSIONS

An unusual derivative of the heat pulse technique has been developed and used to measure the small low temperature heat capacities of metallic samples. From a study of the performance of the calorimeters built for the research presented in this thesis, the following conclusions can be made.

The use of He^3 and He^4 heat exchangers provided a reliable method for fast cooling of the calorimeter itself which has the equivalent heat capacity of several moles of pure copper (Figs. 2, 3, 4). They also completely avoid the use of exchange gas below liquid nitrogen temperatures.

Three different heat switches of increasing reliability and performance were tested. The switch in calorimeter III, with its high thermal conductance Au-Au contacts, is capable of rapidly cooling the sample yet gives a very small heat input when opened even at the lowest temperatures.

The semi-adiabatic method for thermal isolation of the sample with a rigid nylon support was found to be very practical for measuring samples of small heat capacities which are very sensitive to vibrational heating in adiabatic containers. This method is relatively insensitive to vibrations since the heating rate of the sample can be made either negative or positive by controlling the temperature of the sink to which the sample is weakly connected. Using the same procedure, the temperature of the sample can be set to previously established values, which is particularly useful in making determinations of the specific heat in the vicinity of superconducting transition temperatures. The successful operation of this method is due to the relatively large time constant of the associated thermal circuit, which at low temperatures is determined mainly by the large thermal resistance between nylon and copper.

The combination of the three factors mentioned above leads to an effective reduction in the size of the calorimeter. A final improvement can be made by incorporating a continuously operating He^4 evaporator.[23] This could be done easily in Calorimeter III.

During the search for reliable thermometry several resistors were tested as secondary thermometers. An Allen Bradley 15Ω, 1/10 watt, carbon resistor proved to be a sensitive thermometer between 1.4°K and 4.2°K, but its high resistance at low temperatures made it unuseable below 1°K. A Speer 470Ω, 1/2 watt, Grade 1002 carbon resistor was found to be an appropriate choice when working from 4.2°K to 0.4°K due to the applicability of its simple interpolation function suitable for use with desk calculators. However, its sensitivity is relatively low. Finally, the more sensitive and more reproducible germanium resistors were used in calorimeters II and III. A Cryocal 250Ω resistor was used mostly in the experiments presented here.

Considerable problems were found when calibrating the resistors in calorimeters I and II due to the difficulty in obtaining a good equilibrium between the thermometer and the He^4 evaporator where the vapor pressure was measured. Temperature gradients were randomly observed above the lambda point due to oscillations in the evaporator when used as a static container for the vapor pressure measurements. These oscillations were only observed when using a high sensitivity Texas Instrument manometer. Nearly ideal equilibrium conditions were eventually achieved with Calorimeter III in which the helium bulb was placed in the same copper plate as the resistors. This greatly improved the calibration, and smooth fitting of the data

was achieved with a relatively small number of coefficients in the interpolation function.

Finally, the use of an a. c. Wheatstone bridge followed by a recorder proved to be a sensitive and suitable method for the measurement of the thermometer resistance. The nonlinearity effects characteristic of the Wheatstone bridge were avoided by balancing the bridge before and after the heat pulse, thereby recording the temperature drifts in the linear region of the bridge.

TABLE I

Specific Heat Data from Calibration Experiments

Calorimeter	Sample	γ mj/mole°K^2	θ °K
I	0.80 mole "As received" from ASARCO	0.74 ± 0.02	343.5 ± 3.0
II	0.80 mole High vacuum annealed	0.697 ± 0.003	340 ± 2
	5 moles Reference sample[11]	0.694	345.4

FIGURE 1

(a) Adiabatic sample suspension

1) Vacuum jacket

2) Thermal link for the contact

3) Sample

4) Mechanical heat switch

5) Nylon threads

(b) Semi-adiabatic sample suspension

1') Vacuum jacket

2') Thermal link for the contact

3') Sample

4') Driving rod for the contact

5') Rigid nylon support

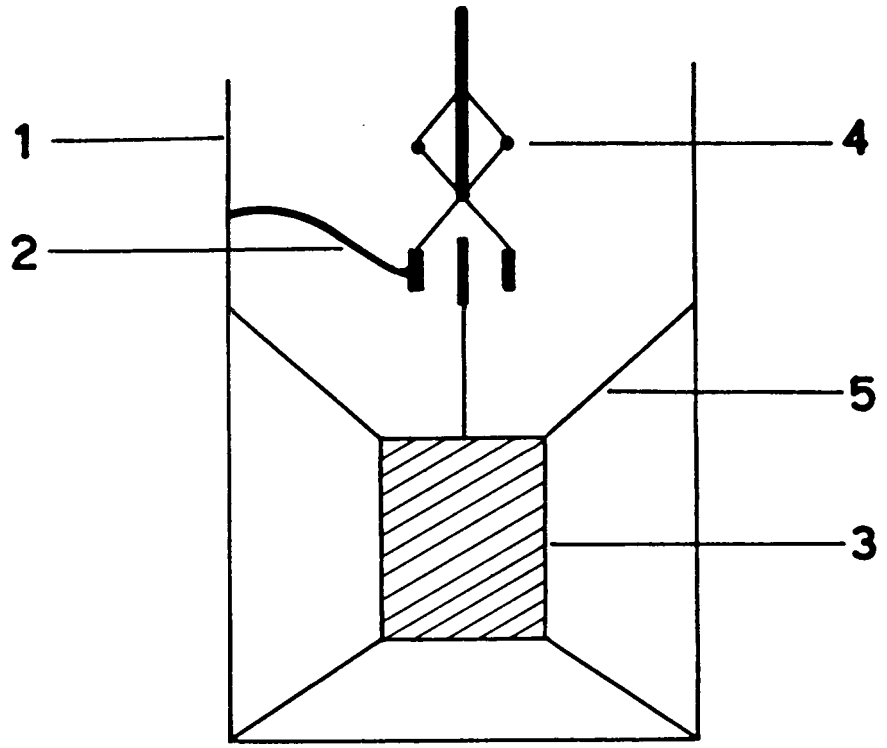

(a)

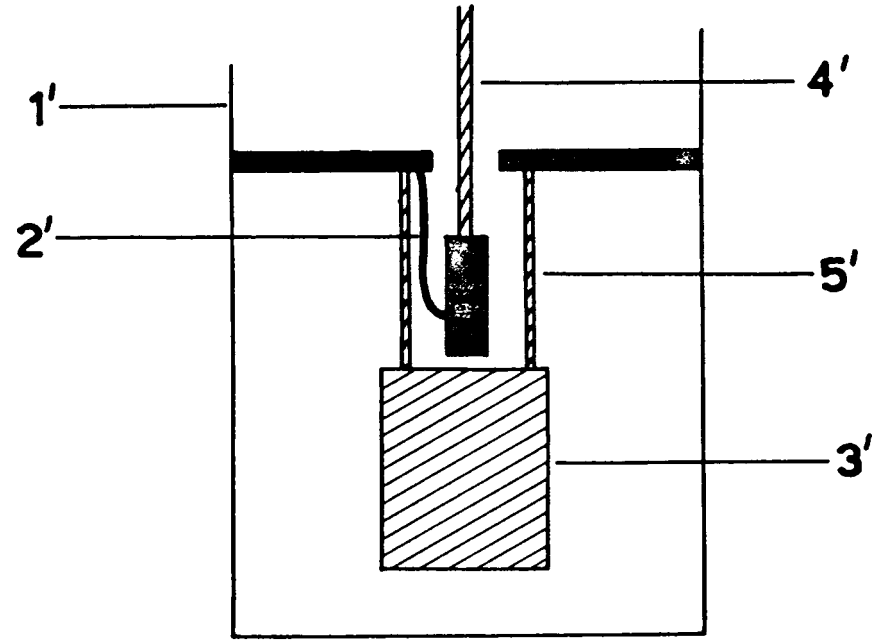

(b)

FIGURE 2

Calorimeter I

a) He^4 refrigerator

b) He^3 refrigerator

c) Temperature controlled shield

d) Carbon resistance thermometers

e) Sample

f) Nylon screws for sample thermal isolation

g) Copper foil for thermal contact

h) Thermal sink

i) Nylon rod

j) Bellows activated by He^4 pressure

k) Rigid nylon cell

l) Thermal and mechanical link for the bellows

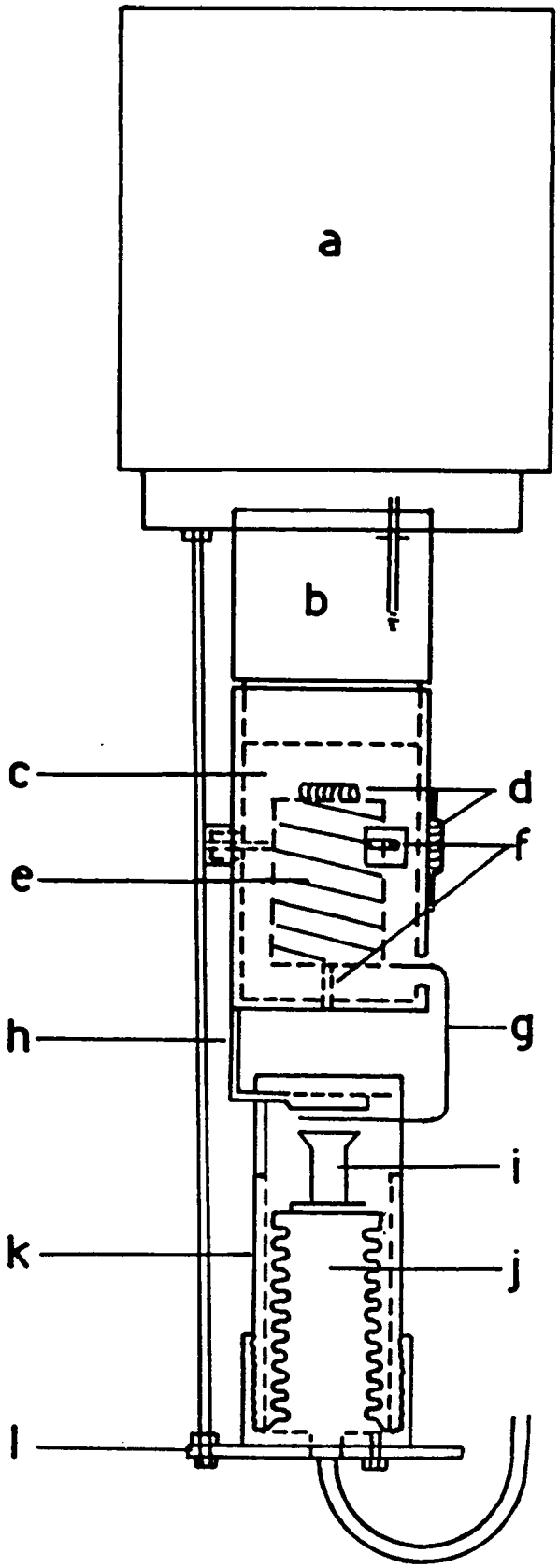
a
b
c
d
e
f
g
h
i
j
k
l

FIGURE 3

Calorimeter II

A) He^4 refrigerator

B) He^4 heat exchanger

C) He^4 high pressure line

D) He^3 refrigerator

E) Thermal and mechanical link for the bellows

F) Heat switch bellows

G) Heat switch nylon driving rod

H) Copper cylindrical guide for G

I) Thin walled nylon thermal insulator

J) Thermal contact

K) Germanium thermometer

L) Copper-berillium spring

M) Shield heater

N) Sample heater

O) Sample

P) Gold plated copper addenda

Q) CMN thermometer

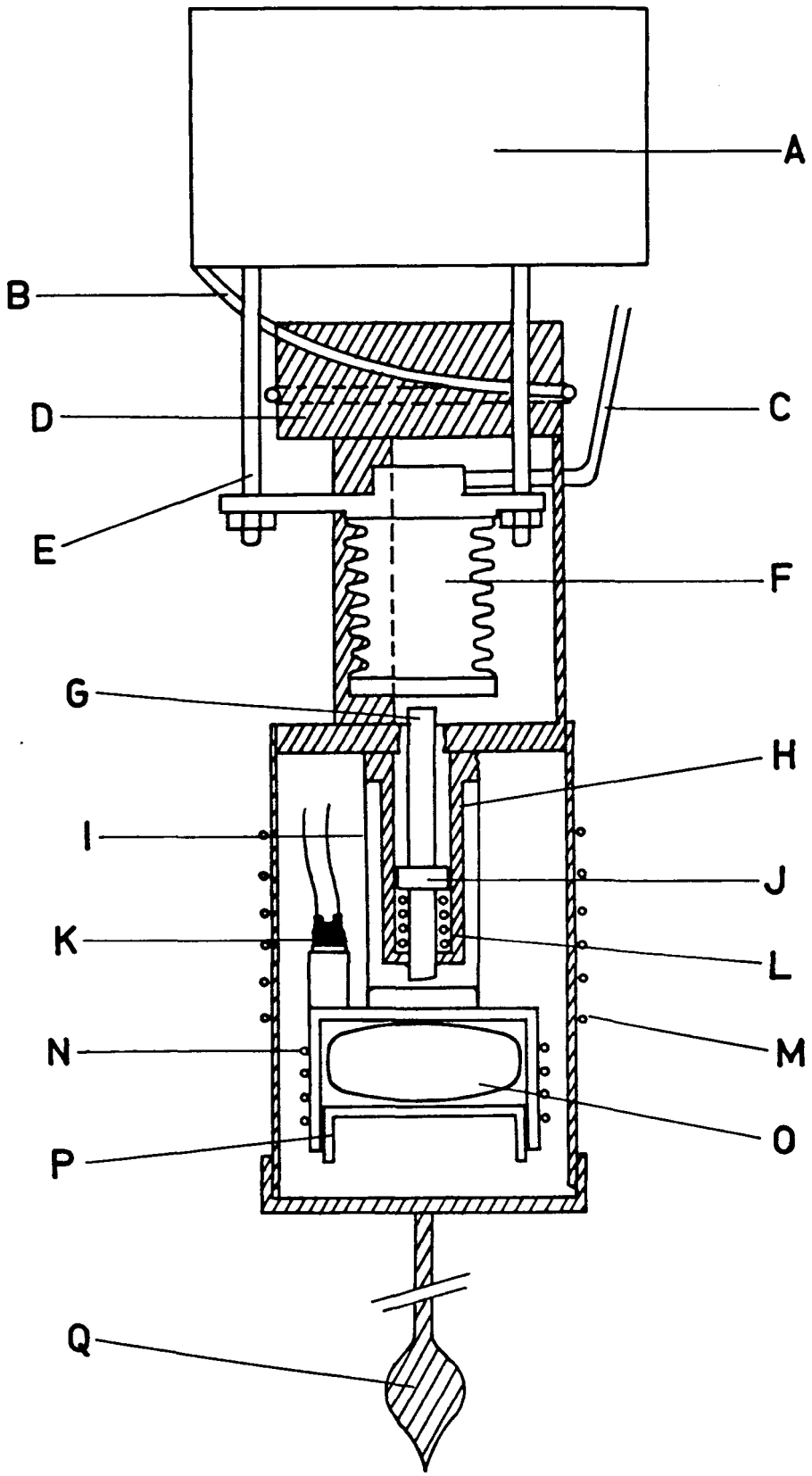
A
B
C
D
E
F
G
H
I
J
K
L
M
N
O
P
Q

FIGURE 4

Calorimeter III

a) High pressure air line

b) Heat switch bellows

b') Heat switch bellows

c) He^3 pumping outlet

d) He^3 return line

e) Manometers line

f) Upper flange for the He^4 dewar

g) Thermal contact driving tube

h) He^3 condenser

i) Vacuum jacket

j) Copper nickel capillary tube 1/64" I. D.

k) Helium bulb for vapor pressure measurements

l) He^3 refrigerator

m) Temperature controlled shield

n) Nylon insulator cylinder 0.005" wall

o) Gold plated copper thermal contact

p) Germanium thermometer

q) Heater and gold plated copper addenda

r) Sample

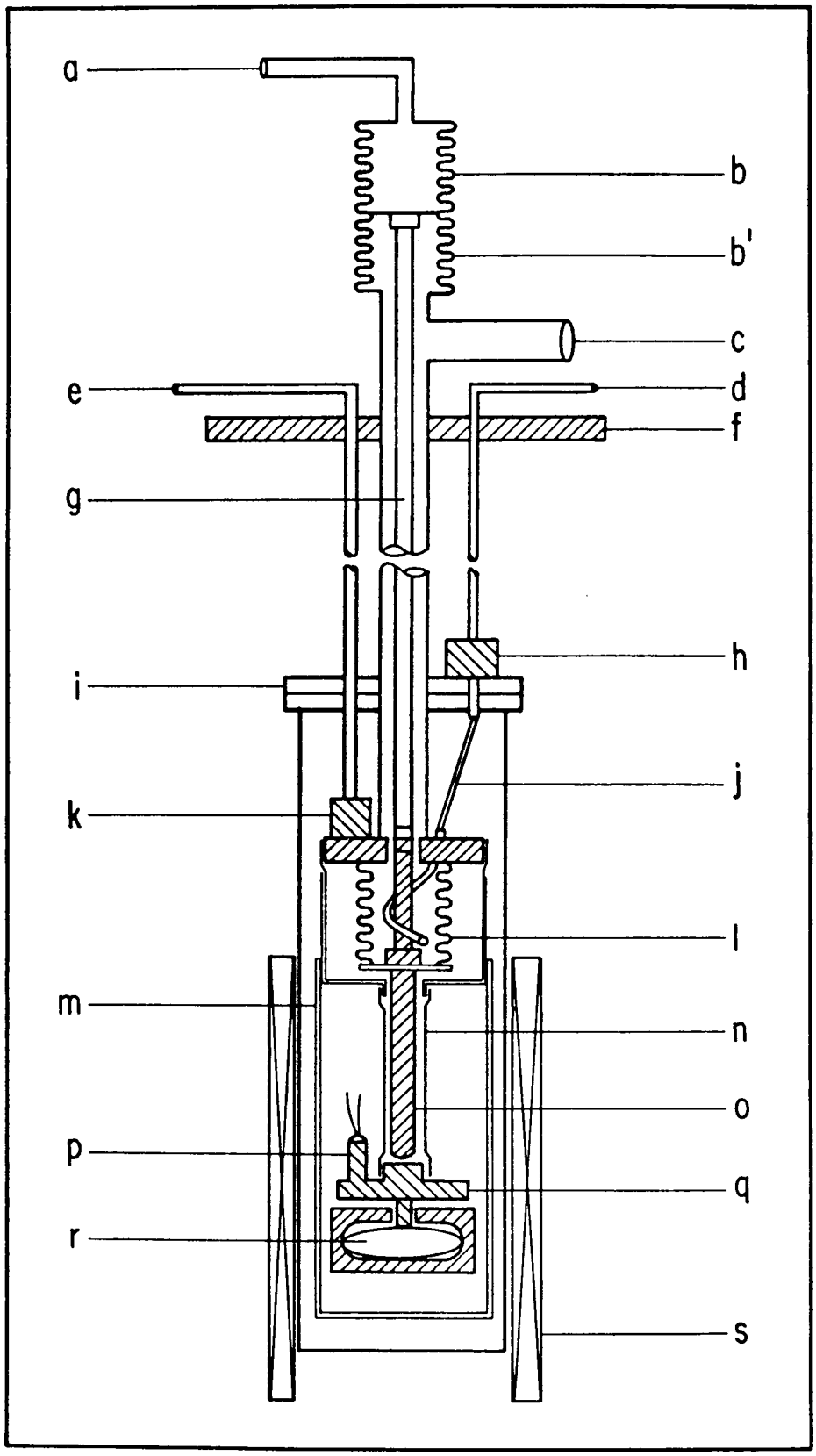
a
b
b'
c
e
d
f
g
h
i
j
k
l
m
n
o
p
q
r
s

FIGURE 5

Typical heat capacity determination (the bridge was balanced before and after the heating interval).

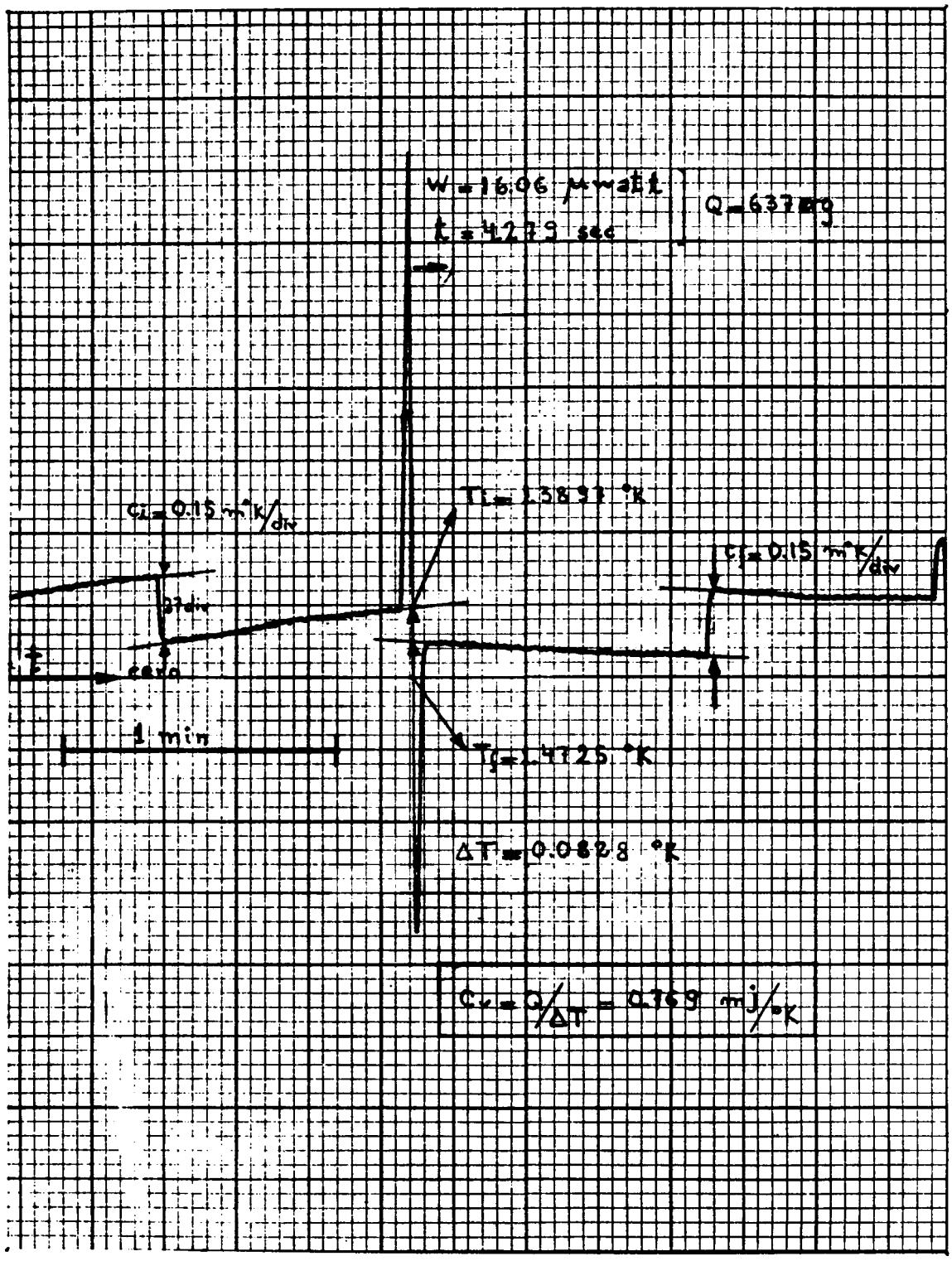
W = 16.06 mwatt
t = 4279 sec
Q = 637 mJ
C_L = 0.15 mJ/°K/div
T_i = 1.3891 °K
C_L = 0.15 mJ/°K/div
37 div
1 min
T_f = 1.4725 °K
ΔT = 0.0828 °K
$C_v = Q/\Delta T$ = 0.769 mJ/°K

FIGURE 6

Thermal conductance of several heat switches at low temperatures.

Solid circles - results for Au-Au contacts (this work);

continuous line - brass-gold contacts (this work);

dashed-dotted line - Au-Au contacts (Ref. 8);

dotted line - nylon sample support (calculated with data from Refs. 6 and 7).

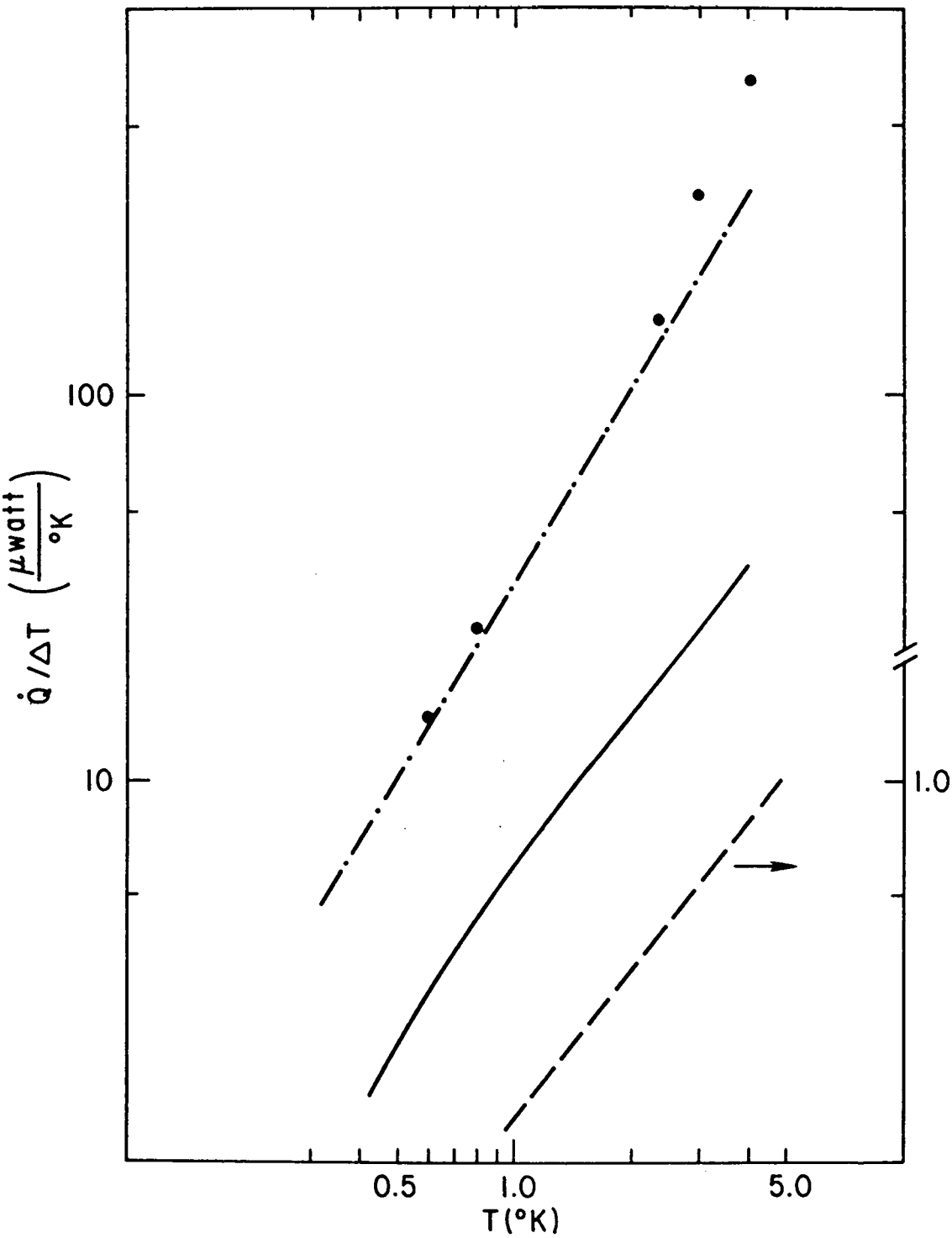
100
10
1.0
$\dot{Q}/\Delta T \left(\frac{\mu watt}{°K}\right)$
0.5
1.0
5.0
T(°K)

FIGURE 7

Deviations from the least squares fitting for the calibration data, obtained for different carbon and germanium resistance thermometers.

a) Allen Bradley 15Ω, 1/10 watt carbon resistance thermometer. Calibrated between 1.4 and 4.2°K against the vapor pressure of He^4.

b) Speer 470Ω, 1/2 watt carbon resistance thermometer, Grade 1002. Calibrated between 0.4 and 4.2°K against a CMN thermometer and He^4 vapor pressure.

c) Cryocal 250Ω germanium resistance thermometer. Calibrated the same way as b).

d) Cryocal 250Ω germanium resistance thermometer. Calibrated between 0.5 and 4.2°K with a helium bulb against He^3 and He^4 vapor pressures.

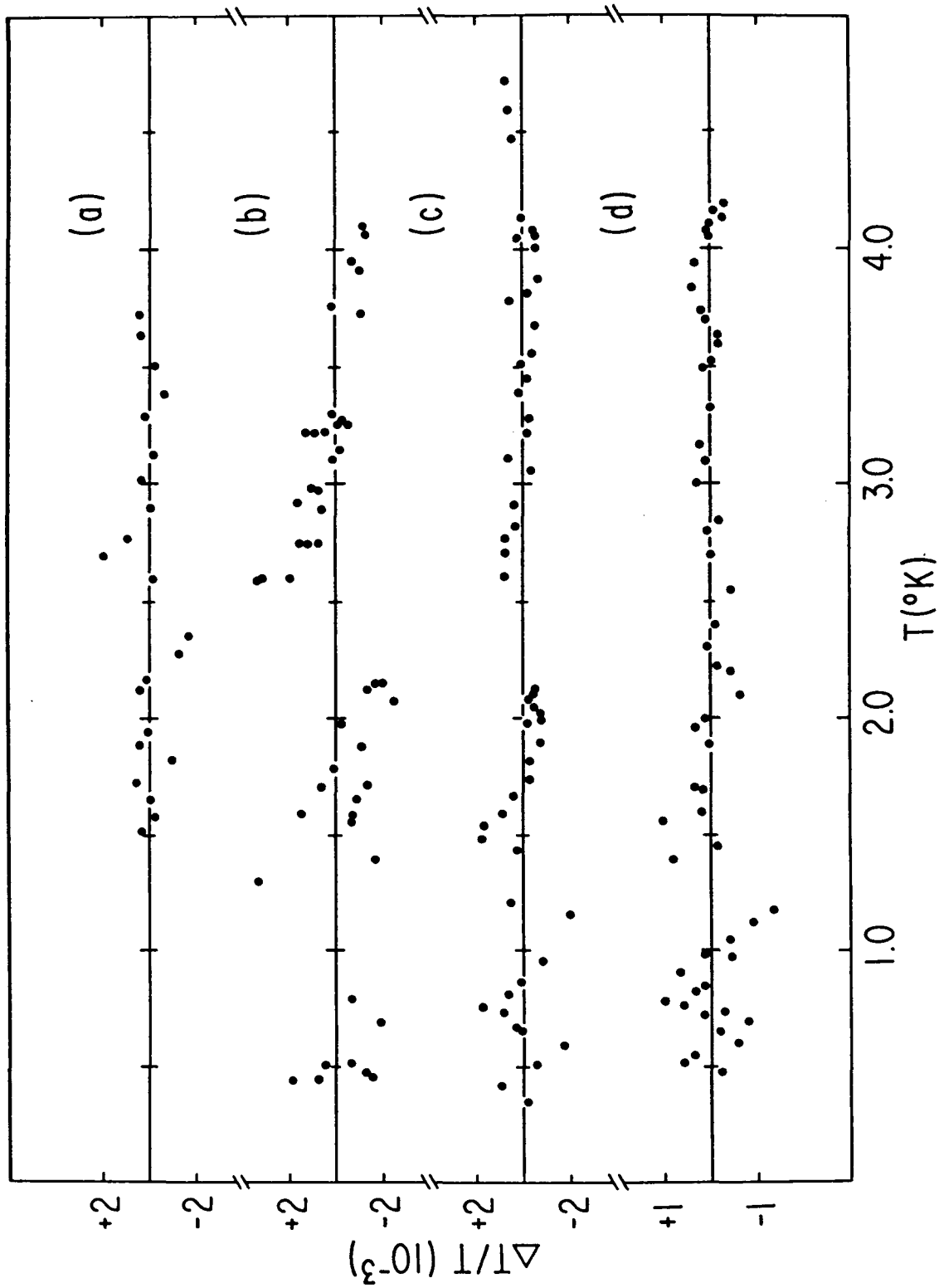
(a)
(b)
(c)
(d)
+2
-2
+2
-2
+2
-2
+1
-1
ΔT/T (10⁻³)
1.0
2.0
3.0
4.0
T(°K)

FIGURE 8

Resistance vs. temperature behavior of the thermometers used in the calorimeters.

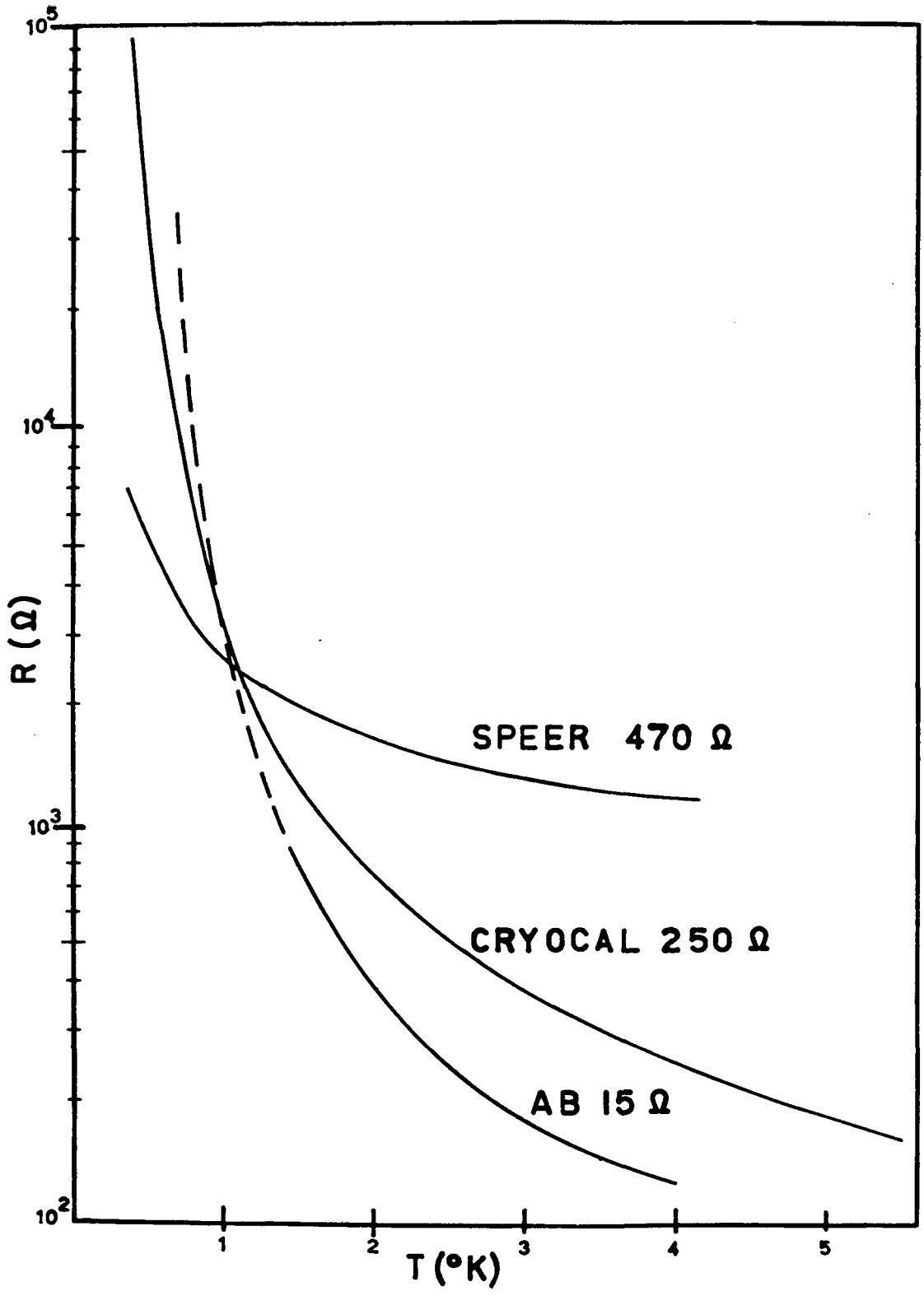
10^5
10^4
10^3
10^2
R (Ω)
SPEER 470 Ω
CRYOCAL 250 Ω
AB 15 Ω
1
2
3
4
5
T (°K)

REFERENCES

1. N. E. Phillips, Phys. Rev. 114, 676 (1959).

2. J. H. Colwell, Rev. Sci. Inst. 40, 1182 (1969); and references therein.

3. K. H. Gobrecht, J. Veyssie, and L. Weil, Proc. of the 1966 Low Temp. Calorimetry Conf., Ann. Acad. Sci. Fennicae A VI, No. 210 (1966).

4. J. P. Abriata, O. J. Bressan, C. A. Luengo, and D. Thoulouze, Phys. Rev. 2B, 1464 (1970).

5. D. Thoulouze, Thesis (unpublished), University of Grenoble, France (1968).

6. A. C. Anderson, W. Reese, and J. C. Wheatley, Rev. Sci. Inst. 34, 1386 (1963).

7. D. F. Brewer, D. O. Edwards, D. R. Howe, and T. E. Whall, Cryogenics 49 (Feb. 1966).

8. R. W. Hill and G. R. Pickett, Ann. Acad. Sci. Fennicae, Ser. A VI, No. 210, 40 (1966).

9. "The 1958 He^4 scale of temperatures," Government Printing Office, Washington, D. C., National Bureau of Standards, Monograph 10.

10. J. E. Vos, Ph. D. Thesis (unpublished), Delft, Holland (1968).

11. D. W. Osborne, H. E. Flotow, and F. Schreiner, Ann. Acad. Sci. Fennicae A VI, No. 210, 35 (1966).

12. J. M. Daniels and F. N. Robinson, Phil. Mag. 44, 623 (1953).

13. W. R. Abel, A. C. Anderson, and J. C. Wheatley, Rev. Sci. Inst. 29, 159 (1958).

14. W. L. Pillinger, P. S. Jastram, and J. G. Daunt, Rev. Sci. Inst. 29, 159 (1958).

15. R. J. Balcombe, D. J. Emerson, and R. J. Potton, J. Phys. E 3, 43 (1970).

16. D. L. Martin, Rev. Sci. Inst. 38, 1738 (1967).

17. G. Cataland and H. Plumb, J. Res. Natl. Bur. Stds. 70A, 243 (1966).

18. Cryocal, Riviera Beach, Fla., USA.

19. M. H. Eldow and H. Plumb, J. Res. Natl. Stds. 70 C, No. 4, 188 (1966).

20. R. H. Sherman, S. G. Sydoriak, and T. R. Roberts, J. Res. Natl. Bur. Stds. 68 A, 579 (1964).

21. Monostat Corporation, N. Y.

22. D. L. Martin, Phys. Rev. 170, 650 (1968).

23. L. E. De Long, O. G. Sympko, and J. C. Wheatley, Rev. Sci. Inst. 42, 147 (1971).